Soil Dynamics and Earthquake Engineering 175 (2023) 108232

Contents lists available at ScienceDirect

Soil Dynamics and Earthquake Engineering

journal homepage: www.elsevier.com/locate/soildyn

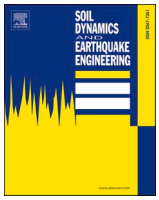

Numerical simulation of SSI free and forced vibration experiments on real scale structures of different stiffness

Marios Koronides [a,*], Stavroula Kontoe [b,a], Lidija Zdravković [a], Athanasios Vratsikidis [c], Dimitris Pitilakis [c]

[a] Imperial College London, United Kingdom
[b] University of Patras, Greece
[c] Aristotle University of Thessaloniki, Greece

A B S T R A C T

Time domain finite element (FE) analysis is a powerful tool for the study of Soil-Structure-Interaction (SSI) phenomena, but it requires a rigorous calibration of all aspects of the numerical model. This study presents three-dimensional (3D) FE analyses that are calibrated and validated against real scale free and forced vibration experiments on the prototype structure of EUROPROTEAS which is founded on soft alluvial sediments. The proposed calibration procedure exploits data recorded during experiments on structures with different structural stiffness, that mobilised SSI effects at different intensities. Particular focus is placed on the modelling of the soil-foundation interface, where zero thickness elastoplastic interface elements are used to allow foundation separation from the soil. A novel approach to simulate contact imperfections (gaps) between the foundation and the adjacent soil is proposed. The results demonstrate the significant impact of the interface gaps and soil nonlinearity on the response of the examined SSI systems, highlighting the importance of a rigorous model calibration.

1. Introduction

Finite element analysis (FEA) is the most rigorous approach to study dynamic Soil-Structure-Interaction (SSI) phenomena. FEA, which is commonly referred to as a direct method, simulates SSI problems in a single step in the time domain, considering the continuous interaction between the structure and the soil. Also, it allows for a rigorous soil modelling, considering soil nonlinearity, soil plasticity, pore water pressure generation, soil stiffness dependence on mean effective stress and other facets of soil behaviour, depending on the soil type and on the adopted constitutive model. These are the main advantages of FEA over other methods that exist in the literature, such as Winkler models [e.g. Refs. [1,2]], lumped models [e.g. Refs. [3,4]] and the substructure method [e.g. Refs. [5,6]]. The disadvantage of FEA is the high computational cost, while the consistent selection of input parameters is one of the main challenges, especially when there is a lack of lab or field data. The uncertainty regarding the input parameters is mitigated when an FE model is validated against real scale experiments, which allow a thorough calibration of the structural, soil and soil-foundation interface properties. However, such numerical SSI studies are scarce in the literature, due to the cost of real scale experiments, as well as the lack of a rigorous numerical procedure for SSI related problems.

Chao [7], Borja et al. [8] and Amorosi et al. [9] developed three-dimensional (3D) FE numerical models to study SSI phenomena observed during seismic events at the Large-Scale Seismic Test (LSST) site located in Lotung, Taiwan. Chao [7] and Borja et al. [8] adopted for the soil a total stress-based bounding surface plasticity model [10], whose parameters were calibrated by exploiting free-field downhole data, as described in Ref. [8]. However, these studies were limited by the inability of the adopted soil constitutive model to predict behaviour at small strains and lack of a complete model validation. Simulating the same experiments, Amorosi et al. [9] developed a 3D SSI model, which was calibrated against one seismic event and was validated against three independent events, ensuring the reliability of the model. The soil domain was simulated with the HSS model [11], extended by Benz [12] and calibrated on site-specific data [7,8]. Pitilakis et al. [13] also employed FE analysis to simulate large scale experiments similar to those of the present study, adopting however a linear elastic soil model. One possible limitation of the above studies is that the anticipated increase of soil stiffness in the vicinity of the foundation due to the existence of the structure [14–17] was not considered.

More importantly, the abovementioned FE studies did not explicitly consider the interface between the soil and foundation. They all assumed full adhesion and bonding between the foundation and the adjacent soil. Such an approximation for the soil-foundation interface model does not allow relative displacements between the two, while it can lead to the

* Corresponding author.
E-mail address: marios.koronides17@imperial.ac.uk (M. Koronides).

https://doi.org/10.1016/j.soildyn.2023.108232
Received 31 March 2023; Received in revised form 1 August 2023; Accepted 4 September 2023

generation of unrealistic effective stresses at the interface. There are various interface models for SSI FE analysis; Herrmann [18] proposed the use of "bond elements" to link the two materials in contact. These are essentially normal and shear springs, which can allow sliding and separation of the two linked materials. Alternatively, finite elements can be placed between the two materials, which, unlike the bond elements, can study the constitutive behaviour of the interface. An approach is to use thin conventional finite elements, behaviour of which is based on standard constitutive laws [19,20]. These elements, though, can cause convergence issues when their aspect ratio is very large and sliding between the two materials is prominent [20]. With respect to the latter, interface or joint elements of either finite or zero-thickness have been widely used for SSI related problems [21–24]. Zero-thickness interface elements have an advantage in that they do not require the calibration of the thickness parameter [20,24], which affects the shear stiffness, mass and damping of a thin interface element [22,23].

The elastic properties of the interface elements are normal (K_n) and shear (K_s) stiffnesses. Due to the lack of lab data, many studies considered arbitrary high values for K_n and K_s [25–28] to restrict elastic relative displacements between the two materials. For the case of a shallow foundation, that is prone to uplift or sliding during dynamic loading, permanent relative displacements between the foundation and the soil can take place, which can be simulated with an elastoplastic interface model [25–28]. It is also crucial that the interface model can simulate the interface contact conditions at rest, as shallow foundations may not be in perfect contact with the soil beneath. Despite this, very few numerical studies in the literature [27,28], have investigated the impact of potential interface imperfections on the SSI response.

This study proposes a rigorous calibration procedure for 3D nonlinear numerical models, which was developed based on the simulation of real-scale free and forced vibration experiments of the EUROPROTEAS prototype frame structure. The developed procedure involves the calibration of the stiffness of the structural elements, the soil nonlinear properties and the interface properties; all verified against a separate series of experiments which mobilise a wide range of strains in the surrounding soil medium. This study also places particular emphasis on the modelling the soil-foundation interface, which is one of the main challenges in numerical SSI studies. A novel approach to model potential interface imperfections is proposed, aiming to take into account areas where the foundation and the soil are not in contact (gap areas).

2. Experimental campaign

2.1. Structure

EUROPROTEAS (Fig. 1a and b) is a 3 × 3 m in plan and 5 m tall frame structure with steel columns (SHS 150 × 150 × 10 mm profiles with length of 3.8 m each) and a removable cross-bracing system (L-shape 100 × 100 × 10 mm profiles with length of 4.3 m each). It is founded on a surface foundation, consisting of a reinforced concrete slab (9Mgr). The superstructural mass consists of one or two identical slabs (9Mgr or 18 Mgr) with dimensions 3 × 3 × 0.4 m each. Two different structural configurations are examined herein. The first configuration comprises a symmetric fully braced structure with a cross-bracing system at all four

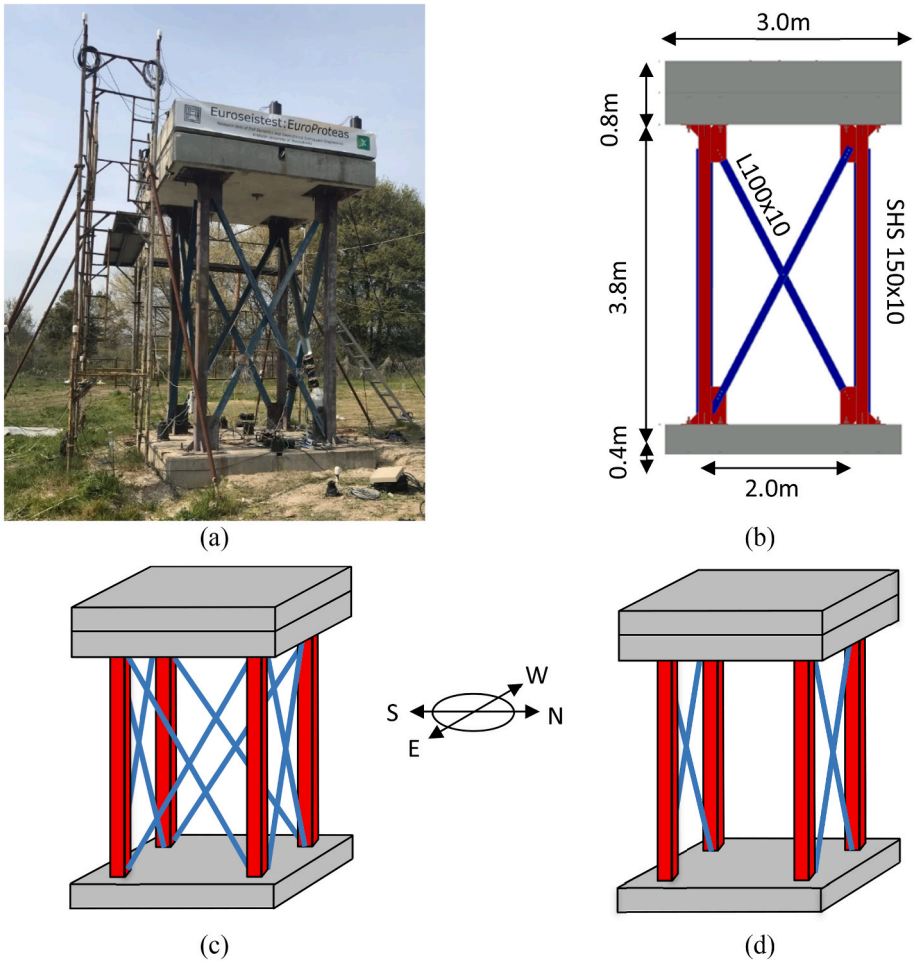

Fig. 1. EUROPROTEAS'S (a) picture, (b) structural elements, (c) fully braced 2-top slab configuration (FBr) and (c) partly braced 2-top slab configuration loaded along its weak plane (PBr).

sides and two top slabs (FBr), as shown in Fig. 1c. The second configuration, shown in Fig. 1d, has two top slabs as well, while it is braced only in the East-West (EW) planes, with reference to the coordinate system shown in Fig. 1c and d. This partly braced configuration, PBr, was loaded along its weak plane which corresponds to the North-South (NS) direction. The examined structural configurations and their characteristics are summarised in Table 1.

The structural design conformed to the provisions of modern codes and regulations [i.e. [29,30]], while it ensured the elastic response of the structural elements during the experiments. The fully braced structural configuration was designed to be very stiff with minimal flexural deformability to allow foundation rocking, as detailed in Ref. [31]. Appendix A presents the calculations of the bearing capacity of the foundation soil as well as the strength properties of the soil. Following the guidelines provided by Eurocode 7 [32], the ultimate vertical force (N_u) is estimated around 8758 kN, while the vertical applied load (N) is 265 kN. Using the closed-form solution provided by Butterfield and Gottardi [33], the moment and shear capacity of the foundation were estimated to be 272kNm and 54 kN, respectively. The design loads for the foundation were a maximum shear force of 50 kN and a moment of 250kNm, which represent the maximum values that could be applied by the available equipment. However, during the actual examined experiments, the maximum shear force and moment that were applied at the foundation level were 15.7 kN and 78.5kNm, respectively.

2.2. Soil conditions

EUROPROTEAS is located at the TST site, the centre of the Euroseistest site, within a valley in Northern Greece. Previous field and lab studies documented the geotechnical properties of the TST site [31, 34–38]. Particular care was taken on the detailed characterisation of the shallow soil layers which are of primary importance for SSI problems [e.g. Refs. [15,17]]. Fig. 2a presents the stratigraphy of the first 30 m of soil, as interpreted from characterisation of samples taken from a borehole drilled below the geometric centre of the foundation [35]. Fig. 2b presents the shear wave velocity (V_s) profiles at the TST site, proposed by previous studies [34–36,38] that interpreted data collected from various techniques mentioned in the figure. The description of these techniques can be found in the referred studies, while a summary of the interpretation process can be found in Ref. [39]. Some of the studies explored the shallow layers of the site [35,38], while others provided V_s profiles that spanned the entire soil column from the surface to bedrock (196 m). The shallow layers are composed of very soft sediments, with estimated V_s values ranging from 100 to 150 m/s at the soil surface, and increasing to approximately 200 m/s at a depth of 15 m. The soil stiffness shows a relatively linear increase with depth, while no significant stiffness contrast is observed between adjacent layers within the first 30 m. During the experiments, the water table was measured in the borehole below the geometric centre of the foundation and found to be 0.8 m below the ground surface.

Soil samples retrieved from borehole drilling were tested in resonant column (RC) and cyclic triaxial (CTX) apparatuses to provide the variations of stiffness and damping ratio with shear strain under cyclic loading (G-γ-D). The locations of samples for which G-γ-D curves are estimated are depicted in Fig. 2a, while more details can be found in Refs. [31,37]. The G-γ-D lab curves were further adjusted to take into account the different conditions existing in the laboratory and in-situ, i.e. loading frequency (f), number of cycles (N) and stress state (p'), that were found to impact the curves [40–42].

Table 1
Structural configurations examined.

Configuration name	Bracing system	Mass (Mgr)	Loading direction
FBr	Full - All four sides were braced	18	NS
PBr	Partly - The North and South sides were braced	18	NS (Weak axis)

The first step of the calibration process involved fitting the Darendeli [42] G-γ-D mean curves to the laboratory data. At this stage the lab conditions were considered; p' was set equal to the mean effective stress imposed in the lab, while f and N were given representable values for RC and CTX tests. Other input parameters such as PI and OCR were available from the lab data [37]. To improve the fitting of the mean G-γ-D curves to the lab data, the statistical Darendeli parameters were adjusted accordingly, ensuring that the resulting curves remained within the $\mu \pm \sigma$ range of the corresponding soil type (where μ and σ are the mean and standard deviation values).

The second step of the calibration involves the computation of the G-γ-D curves using the Darendeli equations with the adjusted statistical parameters of the first stage, considering the in-situ conditions (p', f, N). The mean effective stress of each layer was computed assuming the overburden pressure at the centre of the layer and K_0 conditions ($K_0 = (1 - \sin\varphi') \bullet OCR^{\sin\varphi'}$). The loading frequency was set equal to 1 and number of cycles equal to 10, as these values are commonly used in geotechnical earthquake engineering [40]. Fig. 3 compares the Darendeli curves adjusted for the experimental and in-situ conditions (p', f, N) with the corresponding lab data. These curves pertain to a soil sample retrieved from 2 m depth, as indicated by the first bullet point depicted in Fig. 2a. This soil sample and hence the presented G-γ-D curves are considered representative of the first 3 m of soil, which in the ensuing numerical model is assumed to be the first layer of the soil domain.

2.3. Equipment for excitation load application

2.3.1. Forced vibration

Forced vibration tests were carried out by the means of an MK-500U (ANCO Engineers Inc) eccentric mass vibrator system (Fig. 4a), that can apply horizontal unidirectional sinusoidal forces of various frequencies. It was mounted at the centre of the top slab, which coincides with the centre of mass and rotation of the slab, while it was acting along the NS direction (with reference the coordinate system shown in Fig. 1). This loading configuration ensured that the force was applied along one of the planes of symmetry of the structures, hence minimizing, as possible, the out-of plane (EW) motion.

The vibrator comprises two rotating shafts with eccentrically placed plates, denoted as A, B, C and D, which can be placed with four combinations (mA, mB, mC or mD). The choice of the combination affects the vibrator's eccentricity (E) (see Table 2), which, in turn, regulates the maximum magnitude (F_{max}) of the sinusoidal force according to Eq. (1), as illustrated in Fig. 4b [43].

$$F_{max} = E \times (2\pi f)^2 \tag{1}$$

where, F_{max} is in units of [N], E is in [Kg • m] and f [Hz] is the input frequency to which masses rotate.

2.3.2. Free vibration

Prior to the free vibration of the structures, a static pull-out force was applied incrementally on the top slab along the South direction, with a wire rope-pulling hoist-counterweight system as shown in Fig. 5. The pulling hoist applied a tension force to the wire rope, which was transferred to the top slab as a pull-out force. The force was measured in-situ by a Z-beam tension load cell, which was attached between the wire rope and the top slab. Upon reaching the desired pull-out force magnitude, the wire rope was cut instantaneously (as much as practically possible), allowing the structure to oscillate freely until it came to rest.

2.4. Monitoring instrumentation

During the free and forced vibration experiments, the response of the soil-structure system was monitored by a comprehensive

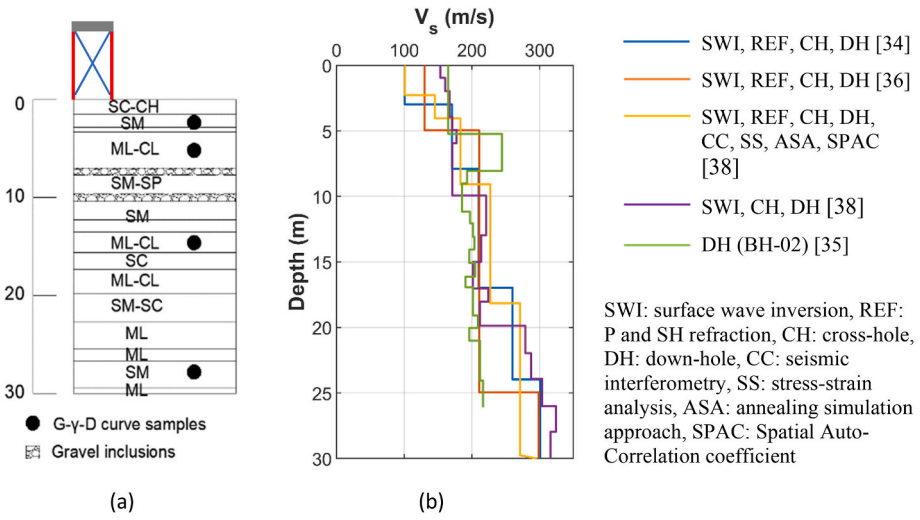

Fig. 2. (a) Soil stratigraphy [35], (b) V_s at the TST site, as interpreted from different tests by previous studies.

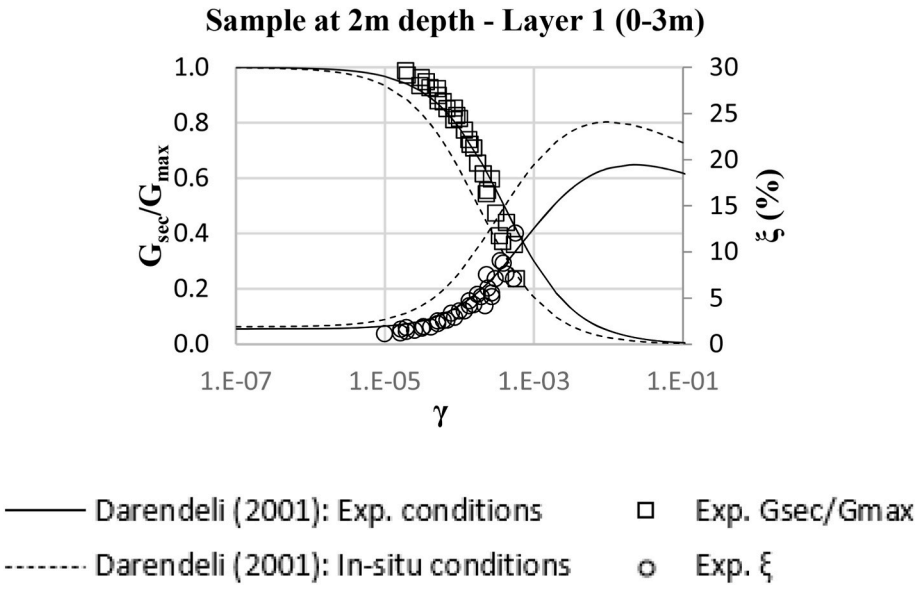

Fig. 3. Stiffness degradation and damping ratio curves, resulting from resonant column and cyclic triaxial tests [31,37] and adjusted Darendeli [42] curves for the experimental and in-situ conditions. The presented data correspond to a soil sample retrieved from 2 m depth and to the first layer of the numerical model.

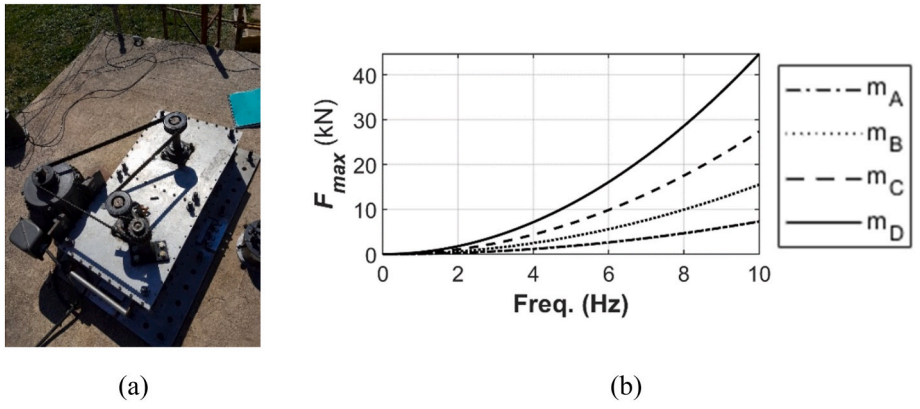

Fig. 4. (a) Vibrator in plan view, (b) magnitudes of the applied sinusoidal force with frequency for each plate combination placed on the vibrator.

Table 2
Total vibrator eccentricity (E) for each combination of plates.

Vibrator mass name	Plates on each shaft	Total eccentricity E (Kg m)
mA	A	1.85
mB	A + B	3.93
mC	A + B + C	6.93
mD	A + B + C + D	11.31

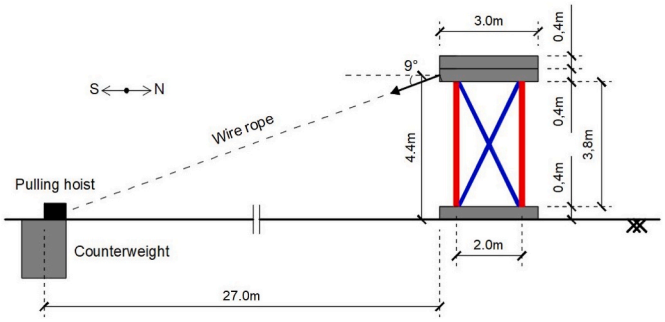

Fig. 5. Schematic illustration of free-vibration system.

instrumentation placed on the structure and the soil surface. In total, there were 9 triaxial accelerometers (4 CMG-5TCDE and 5 CMG-5T type) that monitored the structural response, 13 seismometers (7 CMG-6T and 6 CMG-40 type) that monitored the soil surface motion and one downhole accelerometer (CMG-5TB). The structural accelerometers were mounted on the concrete slabs, the seismometers were buried in a 30 cm deep hole, while the downhole accelerometer was placed in a cased borehole below the geometric centre of the foundation. All instruments were operating at a sampling frequency of 200 Hz and connected to a common global positioning system (GPS) antenna to ensure time consistency and synchronization between each other. For the experiments discussed in this study, the structural and soil instruments were configured in two and three different ways, respectively repeating the experiments. All instrument configurations can be found in Appendix B, while for brevity, Fig. 6 presents one configuration of the structural instruments and one of the soil instruments.

2.5. Experimental imperfections and constraints

Experimental imperfections arise from defects in the geometry of the structure, while additionally, the applied load cannot be perfectly aligned along the plane of symmetry of the structure. Also, although the ground surface was levelled prior to placing the structure into its final position, perfect contact between the foundation and the soil could not be ensured. The uncertainty regarding the soil-foundation interface conditions is compounded by the fact that the reinforced concrete foundation base was pre-cast with a timber formwork supported at two edges only. This process may have resulted in a parabolic foundation base shape due to the compliance of the unsupported formwork. This presumed shape of the foundation base and deviations in the leveling of the ground surface prior to the foundation placement, are expected to form contact imperfections, gaps, between the foundation and the soil. Gaps were also formed beneath the foundation edges as a result of soil densification during the multiple tests that were carried out prior to the examined tests.

Additional sources of experimental imperfections are associated with the column-slab and column-brace connections. The SSI response is expected to be more sensitive to the column-slab connections which carried a substantial proportion of the moment loading that existed during structural oscillation, than the axially loaded column-brace connections. Koronides [39] investigated the moment capacity of the column-slab connections, by exploiting lab data that were obtained prior to the construction of the structure [31]. The lab tests, which are described in Ref. [31], involved static lateral force and free vibration tests on a cantilever structural system. The cantilever consisted of a column that was connected to a rigid base via a bolted connection; both the column and the connection were the same to the ones used on EUROPROETAS. The lab results have shown that the column cannot be considered fixed at the base, instead, it should be considered as a cantilever founded on a rotational spring of stiffness K_θ. However, the scatter seen in the lab tests allowed only to specify a range of K_θ plausible values (i.e. 2465-6400 kNm/rad), while there is no experimental information regarding the stiffness of the column-slab connections of EUROPROTEAS.

In addition to the experimental imperfections, experimental constraints arose due to the unavailability of suitable instrumentation for measuring displacements. The vibratory force was also not measured due to the inherent challenges associated with such measurements, as they have already been established by other forced vibration studies [44,45].

The above experimental imperfections and constraints, which some of them are unavoidable in field experiments, pose significant challenges in developing suitable numerical models. The approach to address the above limitations is discussed in the ensuing sections.

3. Numerical model

3.1. Types of analyses

All numerical analyses were carried out using the Imperial College Finite Element Program (ICFEP) [46]. The analyses simulate free and forced vibration tests on both FBr and PBr structural configurations, with each simulation consisting of both static and dynamic analyses. All analyses start with a Static Self-Weight (StSW) phase which simulates the construction of the structure within one analysis increment, aiming to create the static conditions existing in-situ prior to the application of the external loads on the structure. For the case of the free vibration simulations, the StSW analysis was followed by a second static analysis

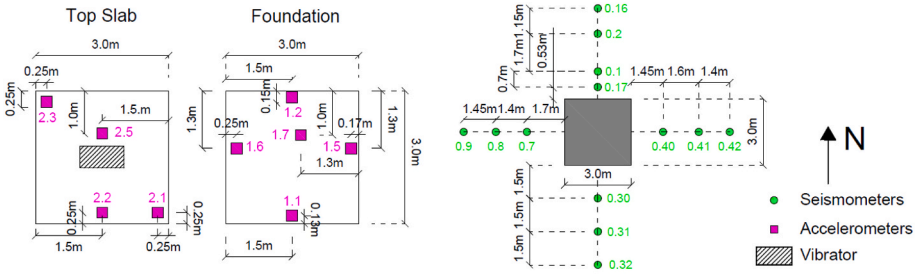

Fig. 6. Plan views of the instrument configurations placed on the (a) structure and (b) soil surface.

phase during which the pull-out force was applied on the structure (StP). Subsequently, dynamic analyses were undertaken, in which the force was removed instantaneously in a single increment, while beyond this increment the numerical model computed the free oscillation of the SSI system. For the simulation of forced vibration experiments, dynamic analyses were carried out directly after the StSW analysis phase. These analyses applied incrementally the vibratory load on the top slab, while computing the SSI response in the time domain.

In all dynamic analyses, the generalized α-integration scheme [47] was used to allow numerical dissipation of the high frequency noise, while maintaining second order accuracy. The input parameter, spectral radius at infinity (ρ_∞), was set equal to 0.818 (9/11), which was found to be the optimum value [48,49]. A full Gaussian element integration was used, as the more computationally efficient 2 × 2 integration led to stress fluctuations and instabilities in the interface elements for the evaluation of, among others, stresses and body forces. The full integration led to 27 (3 × 3 × 3) integration points for the 3-dimensional brick elements and 9 (3 × 3) integration points for the 2-dimensional interface elements.

Preliminary parametric analyses showed that the time step used in the analysis should be smaller than T/20, where T is the period of the applied motion and the predominant period of the structure for forced and free vibrations respectively. Table 3 summarises the time steps used in the numerical analyses which meet the above criterion.

3.2. Problem geometry and boundary conditions

The finite element mesh, dimensions and some of the boundary conditions used for the numerical model are depicted in Fig. 7. Exploiting the symmetry of the problem, only half of the problem geometry was modelled. The dimensions of the simulated soil domain, 15 × 7.5 × 6 m, were decided based on an extensive parametric study, which indicated negligible boundary effects on the structural response and tolerable effects on the soil response for the examined simulations [39]. The soil domain is modelled with 20-noded brick elements and is divided into two layers, to simplify the soil stratigraphy of the site presented in Fig. 2. The spatial discretisation of the brick elements was based on the widely used guidelines of Kuhlemeyer and Lysmer [50].

As only half of the problem geometry is modelled, the displacements perpendicular to the plane of symmetry, u_y (see Fig. 7), are restricted in all analyses. During both the StSW and StP static analyses, the three displacement components of all nodes at the bottom boundary of the soil domain were constrained. The nodes that lie at the lateral boundaries were restricted in the direction perpendicular to the plane of each boundary, as shown in Fig. 7a. These conditions change for the dynamic analyses, except for the nodes at the plane of symmetry which remain unchanged (Fig. 7b). For the dynamic analyses the corner nodes of the bottom boundary of the soil domain are fully fixed, while the cone boundary condition [48,51], consisting of a normal and two tangential springs and viscous dashpots, was applied to the remaining soil boundary nodes, apart from the ground surface and plane of symmetry. The imposition of springs reduces the rigid body movements of the soil domain, which would have occurred at low input frequencies if only the dashpots were imposed [48,52].

Fig. 7c and d presents the structural models of the fully braced 2-top slab and partly braced configurations, respectively. The reinforced concrete slabs, of dimensions 3 × 1.5 m in plan, are modelled with 20-noded brick elements, while the steel columns and braces are modelled with special 3D-formulated one-dimensional beam elements [53] with 3 nodes. A full moment connection was prescribed for the connections between the braces. In contrast, the three displacement degrees of freedom for the connections of the columns with the braces were tied together [46,54], while maintaining free rotation.

The beam elements of the columns were extended into the brick elements of the slab to achieve a moment connection, as shown in Fig. 7c and d. The length of the extended part is equal to the vertical dimension of a brick element (0.20 m) and shares the same nodes with the adjacent brick elements. The twisting degree of freedom of the end node of the extension element is fixed, otherwise the column would be free to rotate torsionally. The stiffness of the connection is determined by the stiffness of the extended beam, whose calibration is discussed later.

Table 3
Time steps used in the forced and free vibration numerical analyses.

Forced Vibration		Free Vibration tests	
Applied frequencies (Hz)	Time step (s)	Structural configuration	Time step (s)
1–2	0.02	FBr	0.01
2–5	0.01	PBr	0.02
5–8	0.005		

3.3. Elastic properties

All structural elements, and for some analyses soil elements too, were assumed to behave as linear elastic materials, with the structural properties selected according to modern regulations, i.e. [29,55]. Table 4 summarises the elastic properties of the structural elements, including Young's modulus (E), Poisson's ratio (ν), density (ρ), cross sectional area (A), moment of inertia (I) and torsional constant (J). The stiffness of the two layers at very small strains were inferred from previous site characterisation studies (Fig. 2b). Table 5 presents the Young's modulus, Poisson's ratio and mass density of the two modelled soil layers.

Material damping for both linear elastic structural and soil materials was represented in the form of Rayleigh damping, following Woodward and Griffiths [56], employing, in the calculations, the smallest and largest resonance frequencies excited during the experiments. The identified frequencies as well as the adopted target damping ratio are shown in Table 6 for each structural configuration. A target Rayleigh damping (ξ) of 5% was selected for the soil domain for the cases that was modelled as linear elastic material (Table 5).

3.4. Input motion

3.4.1. Pull-out force

In StP analyses the pull-out force is simulated as a point load on the top slab over 25 increments. The force is applied to a node on the top slab that lies on the yz plane and the plane of symmetry, along the y-direction at an angle of 9° to the horizontal plane, as illustrated in Fig. 7a. The magnitude of the applied force is half of the one measured in-situ since only half of the problem geometry is modelled.

3.4.2. Vibratory excitation

A limitation of the forced vibration experiments is that the input vibratory force was not measured in-situ and can only be estimated using Eq. (1), leading to uncertainty regarding the magnitude, frequency content and direction of the force. To alleviate this, recorded motions can be used as input excitation in the numerical model, instead of the estimated force. However, it is well established in the literature [57–61] and verified through the current data [39], that the integration of recorded acceleration data can lead to unphysical estimates of velocities and displacements, rendering them unsuitable for direct use in the numerical model. Assuming zero permanent displacements, Koronides [39] developed an integration procedure to overcome this issue which results in reasonable estimates of displacement time histories that can be used as input excitation in the forced vibration simulations.

Therefore, the input excitation was specified in the form of displacement time histories interpreted from accelerations recorded on the top slab by the instrument nearest to the vibrator (this instrument is denoted as 2.5 with reference Fig. 6a). The NS and vertical displacement components were imposed along the x and z-directions of the numerical model, respectively, to the node that corresponds to the position of this

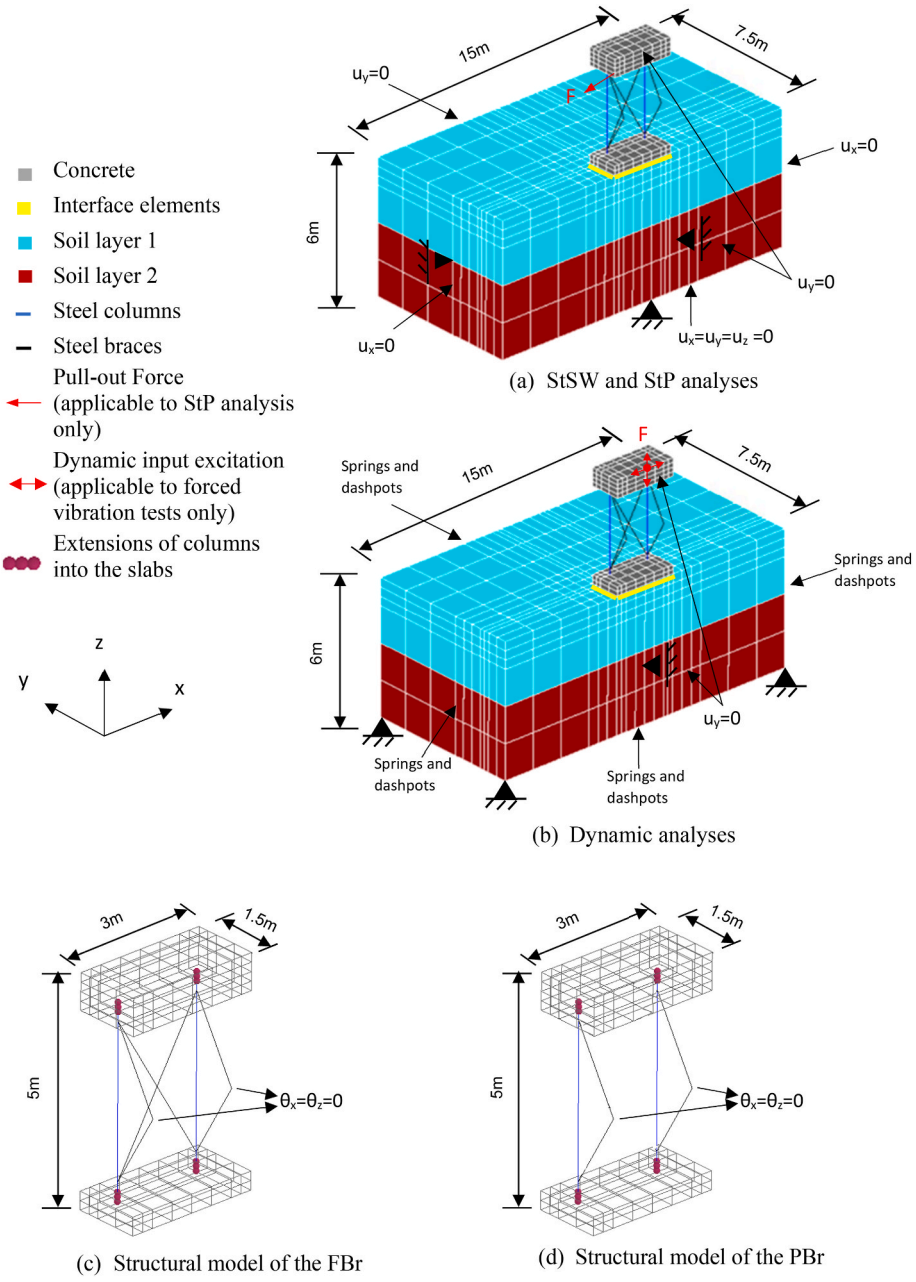

Fig. 7. FE mesh, dimensions and some boundary conditions of the (a) static self-weight and pull-out analyses, (b) dynamic analyses, (c) structural model of the fully braced configuration, (d) structural model of the partly braced configuration.

Table 4
Elastic properties of the structural elements.

	E (GPa)	ν	ρ (Mgr/ m^3)	A (cm^2)	I (cm^4)	J (cm^4)
Concrete	31	0.2	2.5	–	–	–
Braces	200	0.25	7.85	19.2	177	6.97
Columns	200	0.25	7.85	54.9	1770	2830
Beam elements extended into the foundation and top slab	tbc	0.25	0.05	54.9	1770	2830

Table 5
Elastic soil properties.

	E (MPa)	ν	ρ (Mgr/ m^3)	ξ (%)
Layer 1	100	0.25	2.0	5%
Layer 2	186	0.2	2.1	5%

Table 6
Frequencies used for the calculation of Rayleigh damping.

Structural Configuration	F_1 (Hz)	F_2 (Hz)
FBr	3	8
PBr	1	7

instrument. The input motions were tapered for approximately 0.5 s, to achieve a smoother SSI response. The input motion typically included 10–15 cycles, resulting to a steady state response of duration equivalent to 7–12 cycles.

3.5. Interface model

3.5.1. Interface elements

Simulation of the interface between surface foundations and soil to allow the foundation uplift and sliding is a key challenge in SSI problems. For this purpose, zero thickness interface elements available in ICFEP [24,62] were employed (see Fig. 7a and b). The elastic properties of the interface elements are the normal (K_n) and shear (K_s) stiffnesses, which relate the elastic normal (ε) and tangential (γ) interface strains with the normal (σ) and shear (τ) stress. As strains are interpreted in terms of relative displacements (between the two sides of an interface element) normal and tangential to the interface plane, respectively, they have a unit of length, while their stiffnesses have units of kN/m^3.

Similar to Potts and Zdravkovic [63], Koronides [39] has shown that K_s and K_n values can significantly affect the response of an SSI system. When the interface stiffness is very low relative to the structural stiffness, then the overall response of the SSI system is controlled by the flexibility of the interface. Ruiz Lopez et al. [64] argued that K_n and K_s should be high enough to prevent overlap between the contacting bodies in compression, while very high values should be avoided as they cause numerical instabilities. Day and Potts [24] have shown, through 2D analyses, that numerical instabilities may arise when either of the two interface stiffnesses is larger than 100E, where E is the Young's modulus of the stiffer contacting material. This is an empirical rule, as direct comparison between interface and solid element stiffnesses cannot be made since they have different units (kN/m^3 for interface elements and kN/m^2 for solid elements). Following this empirical rule and considering that the largest value of Young's modulus for the materials in contact is 31 GPa (corresponding to the foundation slab), a value of $1E8kN/m^3$ was adopted for both K_n and K_s, representing full contact conditions between the foundation and the soil under compressive normal stress.

To simulate foundation uplift and sliding, an elastoplastic Mohr-Coulomb (MC) model, which can be found in Ref. [24], is introduced for interface elements. The model is characterised by the angle of shearing resistance $\varphi' = 30^o$, cohesion $c' = 0$ and angle of dilation $\nu = 0^o$. Below the MC yield surface, the interface behaviour is governed by its elastic properties. When the stress state reaches the yield surface, K_s switches to zero allowing sliding to occur, while K_n remains unchanged. On the other hand, if foundation rocking is prominent, the initially compressive interface normal stress will reduce in part of the foundation and when it exceeds the tensile strength, set as $c'/\tan\varphi'$ (equal to zero in this case), those interface elements will open, allowing the foundation to rock and part of it to detach from the soil. While interface elements remain open, both shear and normal stiffness switch to zero, while the normal and shear stress remain at $c'/\tan\varphi'$ and zero, respectively. At the same time, normal strains corresponding to the amount of interface opening are accumulated in the plastic hardening parameter (representing the plastic part of normal strains). When the loading conditions change in a way that forces the opening to reduce and eventually close, the plastic hardening parameter reduces and becomes zero upon full closure of the interface opening. At that stage the normal and shear stress start to change again and interface regains its elastic stiffness. During free and forced vibration simulations, some interface elements open and close at different increments, which is enabled by a contact-tracing algorithm in ICFEP [46]. The adopted interface modelling was shown appropriate for the examined structural configuration where sliding is not important but rocking is prominent, in agreement with the claim made by Gazetas et al. [25] for slender structures.

3.5.2. Simulation of gaps

During the field experiments and under static loads, gaps between the foundation and the soil beneath were visually noticeable below foundation edges. Herein, a novel approach to initiate gaps between the foundation and the soil is proposed, using the above MC model formulation for interface elements. As briefly discussed in Koronides et al. [27], the proposed formulation initiates a detachment (gap) of the surface foundation from the soil by initiating the analysis with a non-zero value for the previously mentioned hardening parameter of the model.

The procedure that is proposed to model gaps consists of three main steps. In the first step, the non-contact areas and the magnitude of opening (g) are chosen (both parameters require calibration, see 5.3). The second step requires the initiation of gaps for the StSW analysis by prescribing a relatively large value of hardening parameter for the integration points of the elements where gaps are intended. It is noted that at this stage, the magnitude of opening is larger than g, while it should be large enough to ensure that the initially open gaps will not close due to the self-weight by the end of the StSW analysis. The target interface condition at the end of the StSW analysis is zero stresses at the interface elements that are intended to be initially open. In the final step of the process, in the analysis that follows the StSW analysis, the magnitude of the open integration points is re-defined to be equal to g. This step is performed prior to conducting the StP analysis for free vibration simulations and dynamic analysis for forced vibration simulations.

The adopted name conversion for analyses which employ elastoplastic interface elements and define initial gaps at the interface is EPint_gmm, where g is the magnitude of gap in mm units. For simplicity, EPint_gmm analyses are carried out for forced vibration tests only. Table 7 summarises the analyses that are presented herein, also showing the initial gap magnitudes prescribed prior to the StSW and dynamic analyses.

This study compares the impact of three assumed gap configurations, which are prescribed at the soil-foundation interface prior to the excitation force as shown in Fig. 8. The gap configuration 1 and 2 (GC1, GC2), shown in Fig. 8a and b, simulate gaps at the edges of the foundation; however, they differ in terms of the total area of gaps. The non-contact area of GC3 was prescribed along an interior line of interface elements, as shown in Fig. 8c.

3.6. Soil constitutive behaviour

For the static (StSW and StP) phase of the analyses drained conditions were assumed, implying no change in pore water pressure in the ground (i.e. instantaneous drainage) due to the building self-weight. In the subsequent dynamic phase of the analyses, the soil below the ground water table (at 0.8 m depth) was assumed to behave in an undrained manner. In all analyses, soil is assumed as elastic. Although displacement measurements were not available, permanent settlements or rotations are expected to be negligible due to the weak amplitude of excitation loads. As it can be inferred from Appendix A, the maximum moment-shear state of the foundation, that is examined in the present study, is far from the yield surface, hence elastic soil behaviour is expected. To invigorate the elasticity assumption, nonlinear analyses coupled with a plasticity model (Mohr-Coulomb) were undertaken, which showed that soil plasticity was not triggered at any stage of the analyses (these analyses are not shown herein for brevity).

Table 7
Initial gap openings prescribed prior to the StSW and StP analyses.

Analysis name	Gap (g) opening (mm)	
	StSW	Dynamic
EPint_0.05 mm	2	0.05
EPint_0.1 mm	2	0.1
EPint_0.2 mm	2	0.2

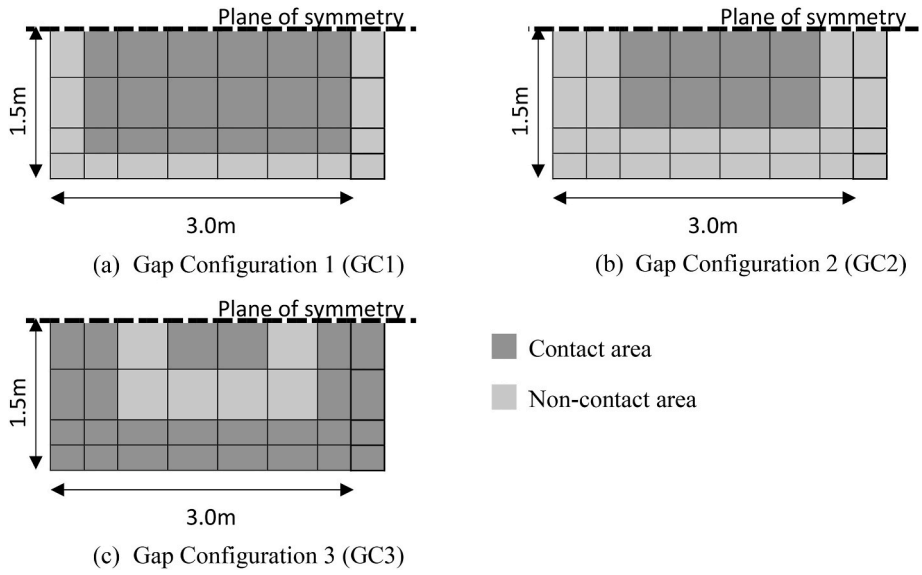

Fig. 8. Plan views of the examined interface contact conditions between the foundation and soil.

The effect of soil's nonlinearity, expressed in terms of a nonlinear elastic stiffness, on the SSI response is investigated. Only a superficial soil layer of 0.8 m thickness is assumed as nonlinear, while the remaining soil domain being linear elastic. Koronides [39] carried out analyses where the whole soil domain was assumed nonlinear, demonstrating that the nonlinearity of the SSI response was controlled by this superficial layer, with the remaining layers mobilising negligible nonlinearity.

3.6.1. Constitutive model

For the nonlinear analyses, the Imperial College Generalized Small Strain Stiffness (IC.G3S) cyclic nonlinear elastic model developed by Taborda et al. [65] was used. The soil shear stiffness at very small strains (G_{max}) is calculated as a function of the mean effective stress (p'), as shown in Eq. (2).

$$G_{max} = G_0 \bullet f_G(e) \bullet \left(\frac{p'}{p'_{ref}}\right)^{m_G} \tag{2}$$

where, G_0 is the magnitude of maximum shear modulus for p' equal to the reference mean effective stress, i.e. atmospheric pressure (p'_{ref} = 101.3 kPa), $f_G(e)$ is a function that incorporates the influence of void ratio on the modulus and m_G is a parameter that defines the nonlinearity of the G_{max} dependency on p'. The influence of void ratio on G_{max} was not considered. The values of m_G and G_0 are selected so that, under free-field conditions, the modelled G_{max} profile approaches the G_{max} inferred from field tests (Fig. 2b). The use of a stress-dependent soil stiffness allows to account for the increase in soil stiffness in the vicinity of the foundation due to the self-weight, which is essential in addressing SSI problems [e.g. Refs. [15,17]]. Eq. (2) implies that stiffness vanishes for zero effective stress, which can be the case for the soil surface. To avoid an unrealistic zero soil stiffness, a hydrostatic suction is imposed above the ground water table. Hydrostatic pore water pressures are also assumed below the water table.

The variation of the tangent shear stiffness (G_{tan}) with the accumulated deviatoric shear strain since the last reversal (E^*_d) is simulated as:

$$G_{tan} = G_{max} \bullet \left(R_{G,min} + \frac{(1 - R_{G,min})}{1 + \left(\frac{E^*_d}{n_G \bullet a}\right)^b}\right) \geq G_{min} \tag{3}$$

where, $R_{G,min}$ is a parameter introduced to limit the degradation of shear stiffness, the parameter a controls the horizontal position of the degradation curve and parameter b controls the degradation rate [66]. The parameter α is dependent on the stress state, while both a and b can depend on the loading direction, which is neglected herein. G_{min} is the minimum shear stiffness beyond which the stiffness does not degrade and n_G is a scaling factor.

Eq. (3) defines the backbone curve when n_G is set equal to one, which is applicable for monotonic loading. On the contrary, n_G changes during cycling loading, taking typically a value equal to two when following the original Masing rules [67,68]. However, it is well established that this value leads to underestimation of damping at small strains and its overestimation at medium to large strains, in comparison with the lab data [65,69–73]. Taborda and Zdravkovic [71] and Taborda et al. [65] proposed the use of a strain dependent scaling factor, as per Eq (4).

$$n_G = \left(d^*_{1,G} + 2\right)^{E^{*d_{2,G}}_d} \bullet \left(\frac{(d_{3,G} + 1) \bullet E^*_d}{1 + (d_{3,G} + 1) \bullet E^*_d}\right)^{d_{4,G}} \tag{4}$$

where, $d^*_{1,G}$, $d_{2,G}$, $d_{3,G}$ and $d_{4,G}$ are model parameters. The overestimation of the damping at larger strains is also mitigated by the imposition of an $R_{G,min}$ value greater than one, in the calculation of G_{tan} (see Eq. (3)) [74,75].

3.6.2. Soil model calibration

The calibration of the IC.G3S model was achieved through a sensitivity analysis, aiming to capture the reference G-γ-D curves and to enable the numerical model to reproduce the experimental results. Specifically, the calibration of the IC.G3S model was based on the adjusted G-γ-D Darendeli [42] curves considering the in-situ conditions (referred thereafter as Reference curves), that are presented in Fig. 3. Previous studies [71–74,76] have shown that when the calibration prioritises a better match of the stiffness degradation curve, this class of models underestimates damping at small strains and overestimates the damping at medium to large strains. In contrast, when the model reproduces the damping ratio curve satisfactorily, the accurate prediction of stiffness is sacrificed. Based on previous experience on site response analyses [72,77] and on preliminary SSI analyses by Koronides [39], it was decided to prioritise the accurate representation of damping. Fig. 9 presents the calibrated secant shear stiffness degradation and damping ratio curves, compared with the reference curves, while the calibrated parameters of the nonlinear model are presented in Table 8.

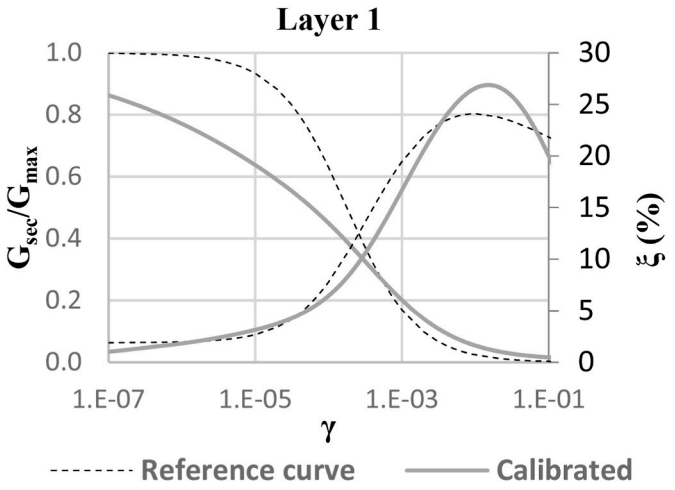

Fig. 9. Reference and calibrated stiffness degradation and damping ratio curves.

Table 8
Input parameters of the nonlinear model.

G_0 (MPa)	88	b_0	0.932	a_2	0.0	$d_{2,G}$	0.001
m_G	0.3	a_0	3.619E-05	$d'_{1,G}$	3.6	$d_{3,G}$	3000.0
$R_{G,min}$	0.008	a_1	0.0	$d''_{1,G}$	0.0	$d_{4,G}$	0.7

4. Modelled experiments and name convention

All modelled experiments exhibited weak out-of-plane motion which allowed their realistic simulation by modelling only half of the problem geometry. Strong motion data, that demonstrate the dominance of the in-plane motion during the simulated experiments, can be found in Appendix C. All simulated experiments and their role as calibration or verification data are summarised in Table 9.

The name convention for the experiments starts with the structural configuration examined (FBr or PBr). This is followed by the magnitude of the pull-out force for the case of free vibration, or by vibrator's rotating mass (i.e. mD) and the input frequency for the case of forced vibration experiments. Structural and soil motions are denoted by the corresponding instrument number shown in Fig. 6, followed by a letter that denotes the motion component. The letter n refers to the NS motion component or the x-direction of the numerical model, while the letter z refers to the vertical component or the z-direction of the model. Herein, the top slab motion will be represented by the 2.5 instrument, the foundation motion by the 1.1 instrument and the soil motion by the 0.1 instrument.

5. SSI calibration

5.1. Procedure

The first step of the calibration process involves the determination of the stiffness of the connections and the structural damping. These properties are calibrated against strong motion data collected during experiments which trigger very weak foundation motion. Such experiments exhibited structural response which can be approximated with fixed-base conditions (i.e. soil is not modelled and fixity conditions are applied below the foundation), and therefore any impact of the soil and interface conditions can be reasonably neglected. The experiment that meets the above criteria is the free vibration test on the partly braced structure for a 2 kN pull-out force (PBr_2.0 kN). Based on this experiment, the Young's moduli of the extensions are calibrated to replicate the natural frequency of the SSI system, while the damping values of all structural elements are calibrated to replicate the amplitude of the response.

At the second step, the interface conditions, including gap configuration and initial opening of gaps, are calibrated, employing a forced vibration experiment that engaged strong foundation uplift for the fully braced structure at an input frequency of 5 Hz (FBr_5 Hz). An advantage of the displacement-controlled forced vibration simulations is that the response of the structure is primarily dominated by the input motion, in contrast with the free vibration response which is strongly affected by the dynamic characteristics of the system. This reduces the relative significance of the adopted soil properties for this type of tests and allows the calibration of the interface model using a linear elastic soil. Additional benefit of forced vibration simulations is that they eliminate the impact of material damping on the response. Chopra [78] has shown that the steady state part of the motion of a single-degree-of-freedom system subjected to forced vibration loading is undamped.

Subsequently, the soil nonlinear constitutive model is calibrated against free vibration tests, which are found to be strongly affected by soil behaviour. The chosen experiments are the free vibration tests of pull-out force equal to 2.9 kN and 15.7 kN on the fully braced structure (FBr_2.9 kN, FBr_15.7 kN). These experiments triggered a relatively wide range of strains in the soil, allowing model's calibration over this strain range. At first, the calibration aimed to replicate the reference curve in Fig. 9, with further refinement where needed to adjust the numerical results to the experimental ones.

It should be noted that each calibration stage is validated against the subsequent stages with further refinements, where needed. The final calibrated SSI model is validated against an independent set of experiments which were not involved in the calibration process.

5.2. Structural properties

The procedure commences by calibrating the Young's moduli of the beam elements extended from columns to the foundation (E_F) and to the top slab (E_{TS}). To simplify the calibration, column-foundation connections are assumed to be rigid, i.e. $E_F = 200E4GPa$, considering that the bolts were regularly tightened during the experiments. On the contrary, the bolts of the column-top slab connections were not inspected frequently, hence E_{TS} is calibrated to account for the compliance of those connections. As earlier explained, the structural properties are calibrated against PBr_2.0 kN free vibration experiment, while assuming fixed-base conditions in the numerical model. Fig. 10 investigates parametrically the impact of E_{TS} on the horizontal top slab motion

Table 9
Simulated experiments.

Exp. Name	Type	Bracing system	Vibr. mass	Freq. (Hz)	Force (kN)	Used for	
						Calibr.	Verif.
FBr_mD_5 Hz	Forced vibr.	Fully braced	mD	5	n/a	✓	✓
PBr_mD_2 Hz	Forced vibr.	Partly braced	mD	2	n/a		✓
FBr_2.9 kN	Free vibr.	Fully braced	n/a	n/a	2.9	✓	
FBr_15.7 kN	Free vibr.	Fully braced	n/a	n/a	15.7	✓	
PBr_2.0 kN	Free vibr.	Partly braced	n/a	n/a	2.0	✓	✓
PBr_13.9 kN	Free vibr.	Partly braced	n/a	n/a	13.9		✓

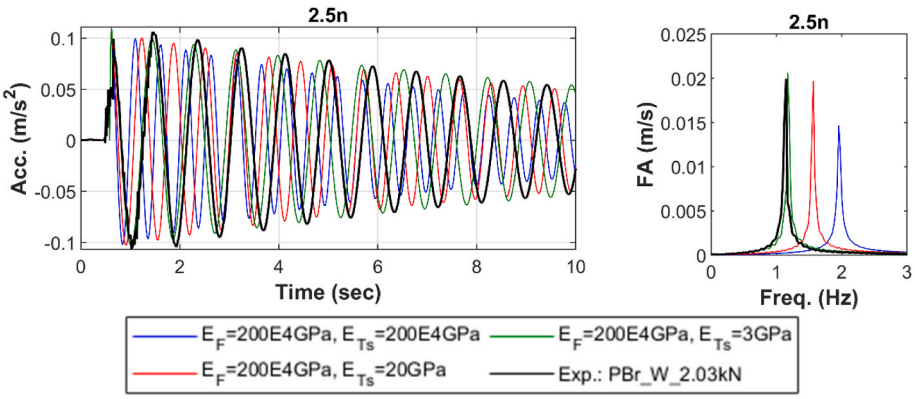

Fig. 10. Calibration of Young's modulus of beams extended into foundation (E_F) and top slab (E_{TS}), by simulating the PBr_2.0 kN experiment and assuming fixed-base conditions.

(2.5n). It demonstrates that the stiffness of the connections affects significantly the natural frequency of the SSI system, as it is clearly indicated by the main peak of the spectra. Assuming a full moment connection, i.e. $E_{TS} = 200E4GPa$, the numerical model predicts a natural frequency that is double the experimental one. The figure demonstrates that $E_{TS} = 3$ GPa is an appropriate value to consider in the subsequent analyses.

In the above analyses, the steel braces and columns were prescribed a 2% target Rayleigh damping ratio, which is typically used for steel structures. A lower value of 1% target damping was assigned to the concrete slabs, as the slabs essentially moved like rigid bodies with negligible bending. The above damping values are deemed suitable, as the motion amplitude produced by the numerical model is in a good agreement with the experimental data. Structural damping was assumed constant throughout the analysis based on the small structural displacements that were observed.

5.3. Interface model

Subsequently the FBr_mD_5 Hz experiment is simulated, assuming linear elastic soil and using elastoplastic interface elements, to calibrate the physical gap opening. For brevity, this investigation is presented only for the GC2 gap configuration (Fig. 8b), which, as it is subsequently shown, was found to be more appropriate than the GC1 an GC3 configurations (Fig. 8a, c). Fig. 11 compares the horizontal and vertical motions of the top slab, foundation and soil, computed by analyses that simulate different magnitudes of gaps (0.05 mm, 0.1 mm and 0.2 mm), initiated prior to the dynamic excitation. The top slab response is

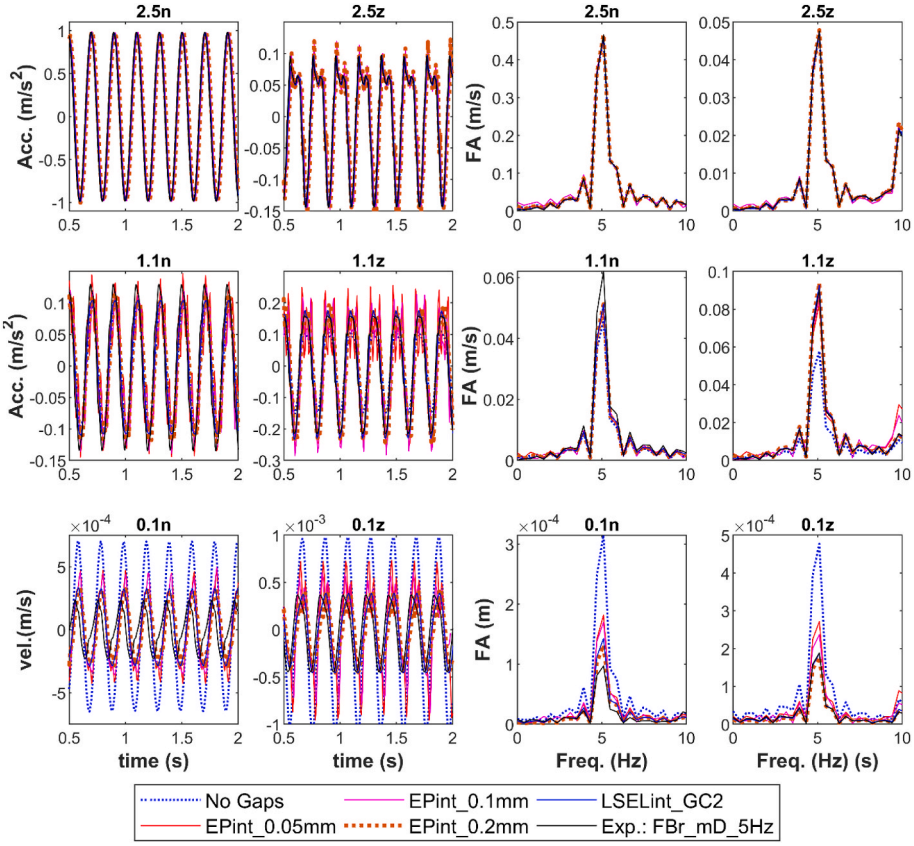

Fig. 11. Impact of the initial opening, prescribed at the initially open interface elements, on the results of the FBr_mD_5 Hz forced vibration simulation, assuming linear elastic soil, GC2 gap configuration and EPint or LSELint gap simulation.

unaffected by the interface conditions, as it is controlled by the input excitation. Analyses without interface gaps underpredict the foundation vertical motions and highly overestimate the soil motion. The vertical motion of the foundation increases and soil motion decreases when gaps are simulated below the foundation edges. These effects are significant even for a very small gap (i.e. 0.05 mm) and become more pronounced for larger openings, approaching the measured response. The EPint_0.2 mm analysis predicts SSI response very close to the field data, implying that a 0.2 mm gap might be appropriate to represent the real conditions.

The EPint analyses can result in high frequency content in the motion, particularly noticeable for smaller gaps, due to the opening and closure of interface elements at different increments. It is observed that the high frequency content is very weak for the EPint_0.2 mm analysis, implying negligible closure of the interface elements that were initiated to be open. Interface elements that remain open throughout the oscillation retain zero stiffness during the entire analysis.

These observations have lead to further study that explored a simplified approach to account for non-closing gaps. The proposal is to adopt elastic interface elements and prescribe low stiffness to those elements representing non-closing gaps (LSELint). Herein, the intended non-contact interface elements are prescribed with stiffness $K_s = K_n = 1E2kN/m^3$, which is much lower than the stiffness of the contact elements ($1E8kN/m^3$). The advantage of the LSELint analysis is that it is less computationally expensive than EPint_gmm analysis. Fig. 11 presents also the response predicted by the analysis that employs LSELint interface elements. This analysis produces results identical with the analysis that initiates with 0.2 mm gaps, further verifying that the initially open interface elements, formed in the latter analysis, do not close at any stage of the motion.

The validity of the adopted gap configuration (GC2) is further investigated through a parametric analysis, which incorporates the three different configurations shown in Fig. 8. For this investigation, the same forced vibration test is simulated, while employing the LSELint to simulate gaps. Fig. 12 shows that gaps simulated below the foundation edges, i.e. GC1 and GC2, increase the foundation motion and decrease the soil motion, with the impact becoming more pronounced for larger gap areas, i.e. GC2. The GC3 analysis, that simulates gaps below the interior of the foundation, and the analysis without any interface gaps predict the same response, indicating that interface gaps at this specific location have a weak impact.

The analysis with the GC2 gap configuration replicates the experimental SSI response sufficiently accurately. As the gap model of the LSELint analysis is more computationally efficient (faster running times), while producing similar results with the more rigorous interface model EPint_0.2 mm, it is used thereafter. This interface model is referred herein as LSELint_GC2.

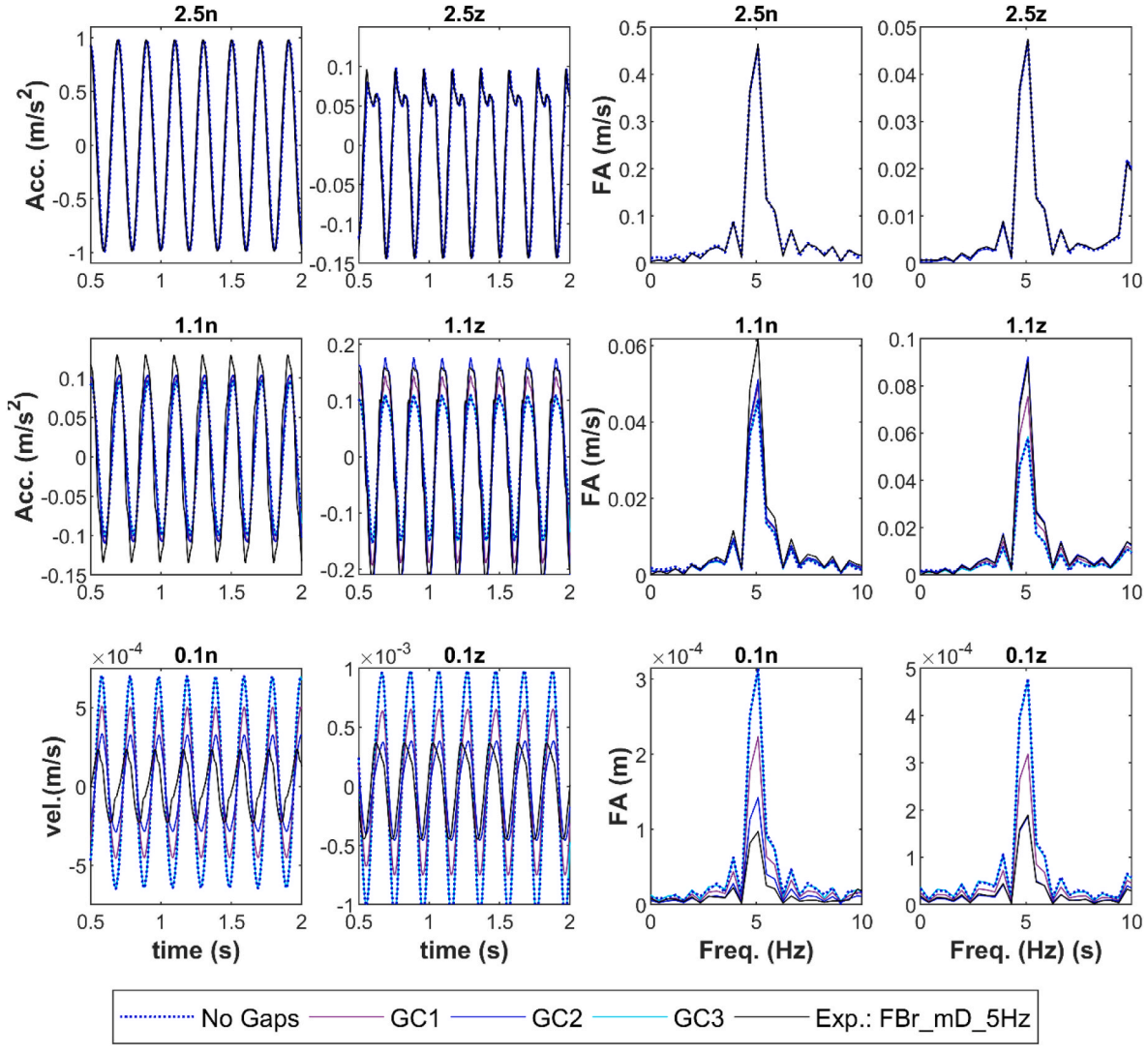

Fig. 12. Impact of the interface gaps configuration on the results of the FBr_mD_5 Hz forced vibration simulation, assuming linear elastic soil and LSELint gap simulation.

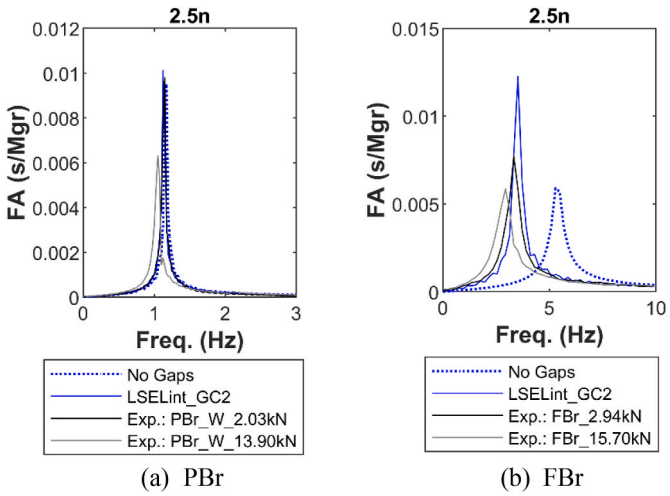

Fig. 13. Fourier spectra of the normalised top slab horizontal motion (2.5n) computed by linear elastic free vibration analyses with and without interface gaps.

Fig. 13 presents the Fourier spectra of the free vibration top slab horizontal motion (2.5n) normalised by the applied pull-out force. This normalisation allows the direct comparison of free vibration responses of different pull-out forces, while any difference between them is attributed to nonlinearities. The figure compares field data against numerical results produced by analyses that do not incorporate any form of modelling interface gaps (no gaps) and analyses with simplified LSELint_GC2 interface modelling. Fig. 13a shows that the simulation of gaps does not make any difference on the free vibration of the partly braced structure. Conversely, interface gaps significantly decrease the calculated natural frequency of the fully braced structure compared to the model without gaps, bringing it closer to the measured frequency and highlighting the necessity of including gaps in the numerical model (Fig. 13b).

As the figure shows, the natural frequency of the two structural configurations is captured well for the free vibration experiments of a small pull-out force, while it is overestimated for the larger forces. Also, with the exception of the PBr_2.0 kN simulation, all simulations overestimate the response of the system. These discrepancies can be attributed to nonlinear phenomena that are not accounted in the specific set of analyses. One source of nonlinearity is interface nonlinearity, i.e. foundation uplift, which however, cannot justify the difference. If the numerical model increases further the foundation uplift, more gapping will take place and hence the motion amplitude will unfavourably further increase. The difference stems from neglection of soil nonlinearity, which would decrease the stiffness and increase damping of the system.

5.4. Nonlinear analyses

Fig. 14 compares results of simulations of different intensity with the LSELint_GC2 interface model and assuming either linear (LINs) or nonlinear (NLINs) soil. The figure presents the Fourier spectra inferred from horizontal and vertical top slab, foundation and soil motions, that have been normalised by the magnitude of the pull-out force. Due to the normalisation, a single LINs analysis can simulate both experiments, while one nonlinear simulation is required for each experiment to account for different levels of nonlinearities. The NLINs analyses incorporate the G-γ-D curve of Fig. 9 in the numerical model.

Fig. 14 demonstrates the significant impact of soil nonlinearity on the SSI response, which becomes more pronounced for the simulation of experiments with larger pull-out force. As expected, nonlinearity decreases the natural frequency of the system due to soil stiffness reduction, as indicated by the shift of the main peak of all motions. It also significantly decreases the amplitude of the motions, which is a consequence of the development of hysteretic damping within the soil in the vicinity of the foundation.

6. Verification

The model calibration is verified against the FBr_mD_5 Hz and PBr_mD_2 Hz forced vibration tests, as well as the PBr_2 kN and PBr_13.9 kN free vibration tests. The following figures compare results of linear and nonlinear analyses with strong motion data. Figs. 15 and 16 present the SSI response predicted by the FBr_mD_5 Hz and PBr_mD_2 Hz simulations, respectively, illustrating the weak impact of soil nonlinearity on forced vibration simulations. Fig. 17 demonstrates that the free vibration response of the partly braced structure is affected by soil nonlinearity, but to a weaker extent than the response of the fully braced structure (Fig. 14). For all simulations, the structural response is accurately predicted by the numerical models. The agreement between the computed soil response and the field data is deemed reasonable,

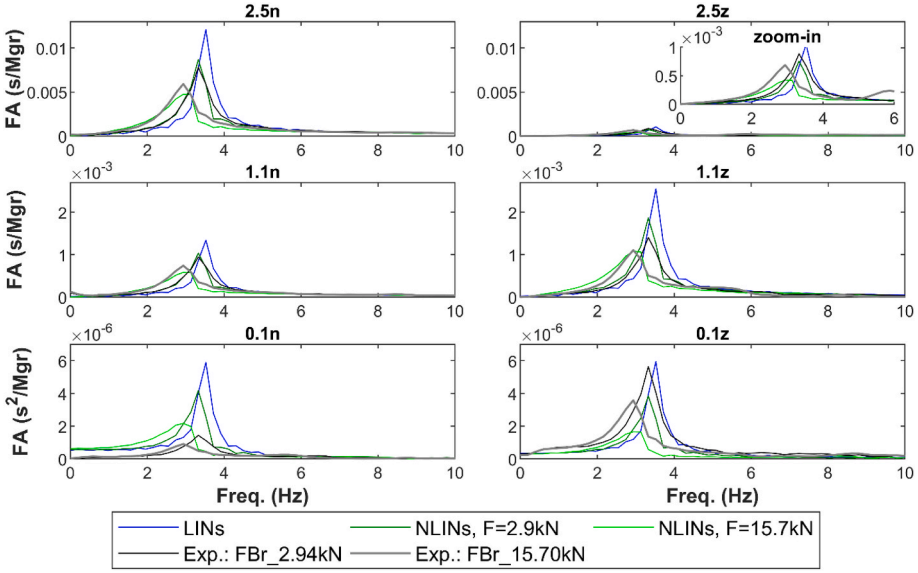

Fig. 14. Impact of soil nonlinearity on the normalised SSI free vibration response of the FBr structure.

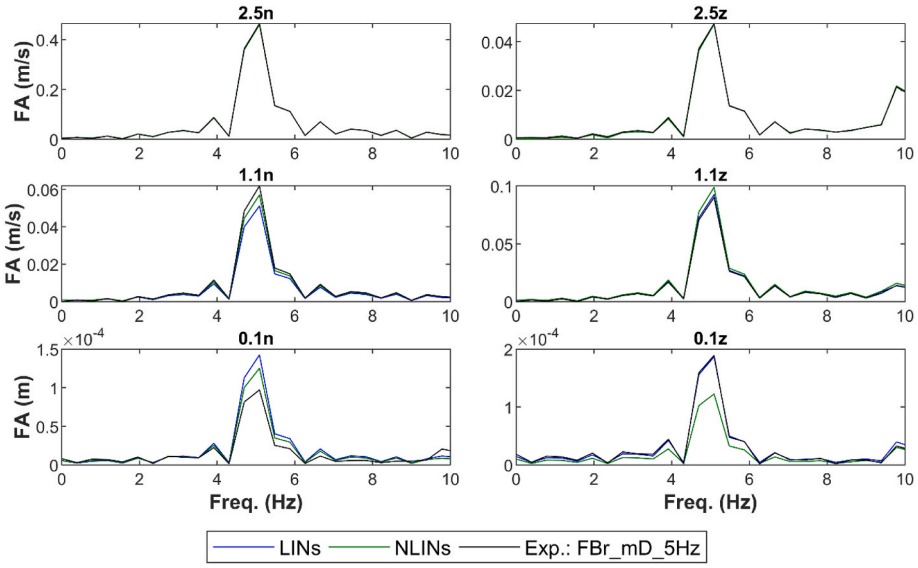

Fig. 15. Impact of soil nonlinearity on the SSI forced vibration response of the FBr structure, when the input frequency is 5 Hz

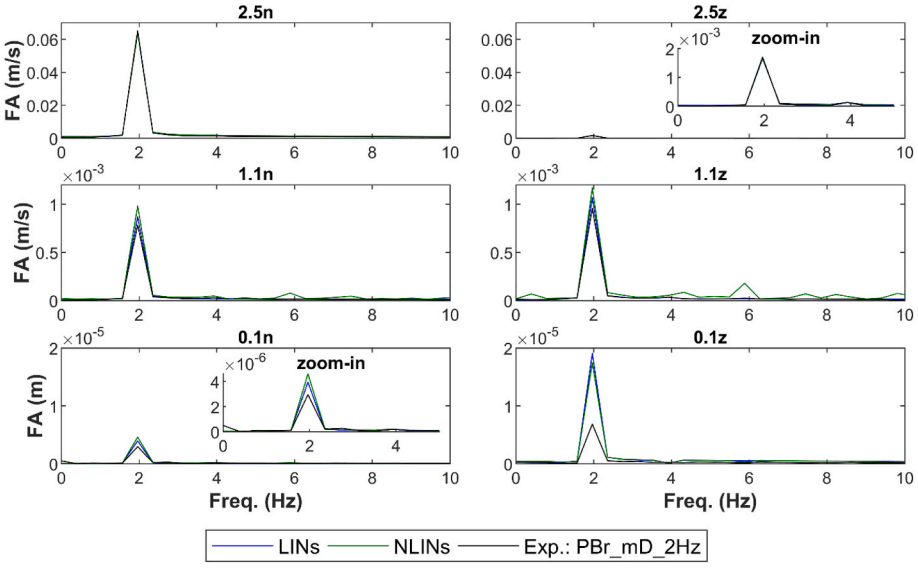

Fig. 16. Impact of soil nonlinearity on the SSI forced vibration response of the PBr structure, when the input frequency is 2 Hz

considering the uncertainties associated with the manual installation process of soil instruments as well as their reliability for low-velocity measurements.

7. Discussion

A foundation with permanent gaps at the interface can be equivalently considered as a smaller foundation in its surface, but with the same moment of inertia. According to Amorosi et al. [9], a smaller foundation amplifies the structural motion and decreases the natural frequency of the system. Gazetas [26] attributes the natural frequency decrease to the increase of foundation rocking that takes place for smaller foundations. The present study verifies the above claims, as gaps between the foundation and the adjacent soil promote a more flexible system and stronger structural excitation (Fig. 13). The decrease of numerical natural frequencies due to the existence of gaps (Fig. 13) can be attributed to the lower contact area at the interface, which reduces the foundation stiffness and consequently the stiffness of the entire SSI system. The motion amplification can be explained by the fact that gaps accentuate foundation rocking, which reduces the ability of the foundation to radiate energy in the soil medium. It is well established [e.g. Refs. [60,79,80]] that the rotational modes of foundation oscillation can radiate less energy to the soil medium than the translational modes. The smaller energy radiation is depicted in the smaller soil motion predicted by analyses with gaps compared to those without gaps, despite that the former analyses predicted a stronger foundation response (Fig. 12).

Strong foundation rocking was found to take place even for a small magnitude of gap initiated prior to the application of the external excitation. In contrast, no foundation detachment took place when gaps were not initiated at the interface. The accumulation of static stresses below the edges of the foundation that exist when gaps are not simulated, do not allow foundation uplift to take place during the dynamic response of system. A small initial gap maintains zero normal stresses at the interface, allowing foundation uplift and re-attachment to take place at several increments of the motion. This observation highlights the important role of static stresses on the behaviour of foundation during dynamic loading. This aspect is discussed in Refs. [39,81], but not elaborated herein. Based on the demonstrated impact of gaps on the SSI

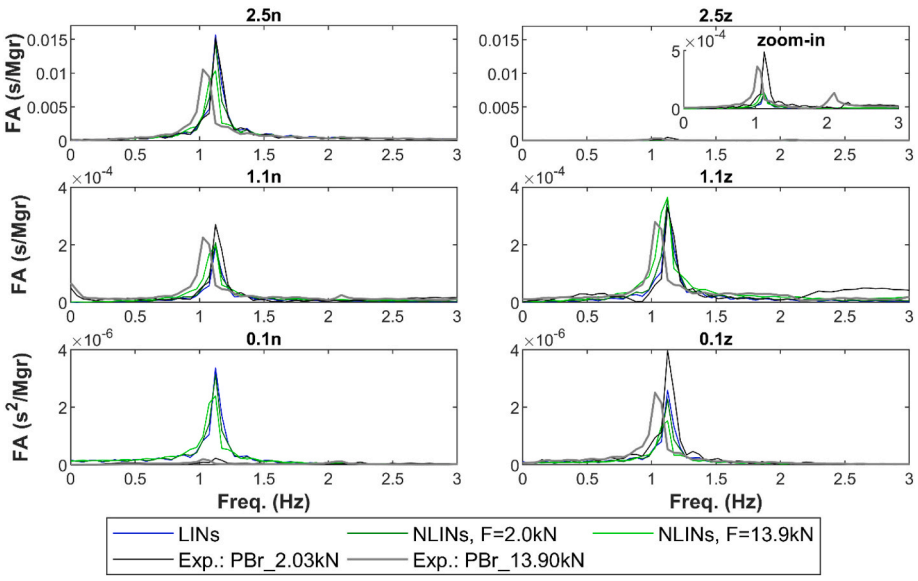

Fig. 17. Impact of soil nonlinearity on the normalised SSI free vibration response of the PBr structure.

response, it is recommended that the presence of any interface gaps beneath prefabricated shallow foundations should be given consideration during the design process.

The numerical results have also demonstrated the important impact of soil nonlinearity on the SSI free vibration response. Soil stiffness degradation and hysteretic damping development decreased the natural frequency of an SSI system and the amplitude of the response, respectively. As expected, the impact was more pronounced for stronger excitation force and for the stiffer structure, FBr, which mobilised stronger soil motion. Nonlinear analyses predicted weaker structural and soil motions than linear analyses, for all simulated experiments. This observation implies that soil nonlinearity produced damping that exceeded the equivalent 5% damping ratio that was incorporated in the linear elastic soil. Considering that only the surficial 0.8 m of soil was modelled to behave nonlinearly, the importance in SSI problems of modelling the soil in the vicinity of the foundation appropriately is highlighted.

8. Conclusions

This paper proposes a rigorous procedure to calibrate a numerical model that simulates real-scale field SSI experiments. The calibration benefits from free and forced vibration experiments that were carried out on different structural configurations, a fully braced and a partly braced configuration. A key strength of the proposed calibration procedure is that it exploits the advantages of each test, allowing the calibration of each aspect separately.

- The structural properties were calibrated against field tests that engaged weak SSI effects.
- The interface conditions were calibrated against field tests that engaged strong foundation rocking but weak soil nonlinearity.
- The soil constitutive behaviour was calibrated against laboratory data and field tests that induced strains of a wide range in the soil.

The above steps of the calibration demonstrate substantial benefits that field tests on different structural configurations and of various excitation loads can bring to the calibration process. Additionally, the step-by-step procedure facilitates a comprehensive understanding of some aspects of SSI simulations that are significant for the accurate prediction of the response. The numerical results have shown that the SSI response can be significantly affected by soil nonlinearity and the presence of gaps between the foundation and the soil, highlighting the importance of modelling these aspects rigorously.

Soil nonlinearity can significantly decrease the natural frequency and increase the damping of an SSI system, with respect to a linear system. These effects have been found to be very prominent on the stiffer structural configuration examined, i.e. fully braced, as opposed to the more flexible configuration, i.e. partly braced. As expected, the stiffer structure engaged stronger SSI effects, resulting in greater strains induced in the soil and promoting soil nonlinearity. In SSI problems where the excitation is induced through vibrations on the structure, soil nonlinearity has been shown to be significant only in the vicinity of the foundation. This observation yields a valuable advantage as it enables the deeper layers to be assumed as linear elastic without compromising the accuracy of both the structural and soil response.

In addition to soil nonlinearity, interface conditions have been shown to exert a significant influence on the response of an SSI system. In particular, this study focuses on the role of interface gaps that can exist between the foundation and the soil under rest conditions. The gaps, even of very small magnitude, were found to significantly decrease both the natural frequency and the damping of an SSI system, in comparison with the counterparts of a system without interface gaps. These effects are attributed to the smaller interface area, which renders the system more flexible and diminishes the ability of the foundation to transmit energy to the soil medium. Given the demonstrated influence of interface gaps on the SSI response, it is recommended that the presence of such gaps beneath prefabricated shallow foundations to be carefully considered during the design process.

Finally, this study proposes a novel approach to modelling initial interface gaps prior to the excitation load, while additional gaps can also be created due to structural oscillation. This approach incorporates plasticity in the constitutive modelling of the adopted zero-thickness interface elements, allowing foundation detachment and rocking motion to be accurately reproduced. For practical use in design, the study further proposes a simplified modelling of interface gaps with elastic interface elements, which was demonstrated to reproduce the SSI response with similar accuracy.

Declaration of competing interest

The authors declare that they have no known competing financial interests or personal relationships that could have appeared to influence the work reported in this paper.

Data availability

Data will be made available on request.

Acknowledgments

The experimental campaign was funded by SERA (Seismology and Earthquake Engineering Research Infrastructure Alliance for Europe). The first author wishes to thank Skempton Scholarship, The A.G. Leventis Foundation and Cyprus State Scholarship Foundation for their support. The vibrator was provided by the Institute of Engineering Seismology and Earthquake Engineering (ITSAK-EPPO) [82], and monitoring instruments were provided by the Laboratory of Soil Dynamics and Geotechnical Earthquake Engineering (SDGEE) of Aristotle University of Thessaloniki (AUTH).

Appendix A. Foundation bearing capacity

The bearing capacity of the foundation to vertical loads is estimated according to the guidelines provided by Eurocode 7 [32]. In this estimation, the presence of moment and horizontal forces was disregarded, while the soil is assumed to have an effective angle of shearing resistance of 30°, cohesion of 10 kPa, and an effective unit weight of 20 kN/m^3. Based on these assumptions, the drained bearing capacity of the foundation soil is calculated to be 973 kPa. For a 3 m × 3 m foundation, the ultimate vertical force is $N_u = 8758$ kN. The applied vertical load (N) is estimated around 265 kN. This estimation takes into account the weights of the two top slabs of the superstructure as well as the foundation slab, with each slab weighing approximately 9Mgr.

The moment (M) and shear (H) capacity of the foundation is determined using the empirically derived N - H – M interaction diagram, proposed by Butterfield and Gottardi [33]:

$$\left(\frac{H}{t_h}\right)^2 + \left(\frac{M}{B \bullet t_m}\right)^2 + \frac{2 \bullet C \bullet M \bullet H}{B \bullet t_h \bullet t_m} = \left[\frac{N}{N_u} \bullet (N_u - N)\right]^2 \tag{A.1}$$

where, $B = 3$ m is the width of the foundation, and $t_h = 0.52$, $t_m = 0.35$ and $C = 0.22$ are parameters whose values correspond to the interaction diagram that provides the best fit to the experimental data. These data were obtained from laboratory experiments conducted on roughened and rigid surface footings placed on dense sand. Naturally the examined configuration does not fully comply with the experimental set up of Butterfield and Gottardi [33], however, Equation (A.1) is sufficient to approximate the load on the foundation with respect to the proposed interaction diagram.

Using the above expression and assuming a constant vertical load (as computed above), the M - H failure envelope for the foundation of EUROPROTEAS is illustrated in Fig. A1. In the examined experiments, the foundation shear and moment forces are related by the equation $M = H \bullet h$, where $h = 5$ m, representing the vertical distance between the load application point and the foundation base. Exploiting this constraint as shown in Fig. A1, the ultimate moment (M_u) and shear (H_u) forces of the foundation are estimated to be 272kNm and 54 kN, respectively.

The maximum horizontal force that can be applied by the vibrator is 50 kN and the maximum examined is 15.7 kN, which result in base moments of 250kNm and 78.5kNm, respectively. These states lie below the yield surface, as illustrated in Fig. A1.

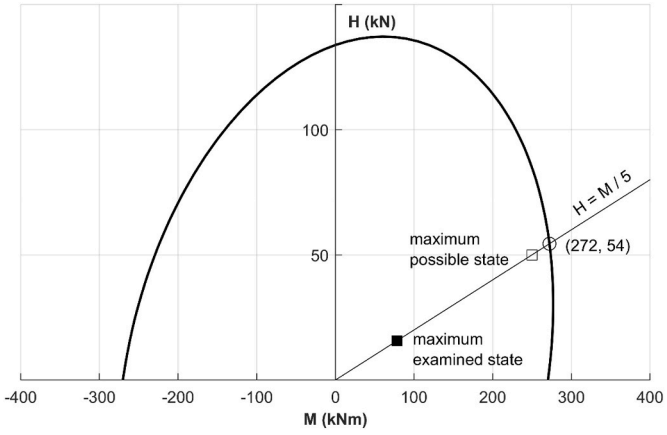

Fig. A.1. Failure envelope in the M –H plane estimated for the case of the EUROPROTEAS'S foundation

Appendix B. Instrument configurations

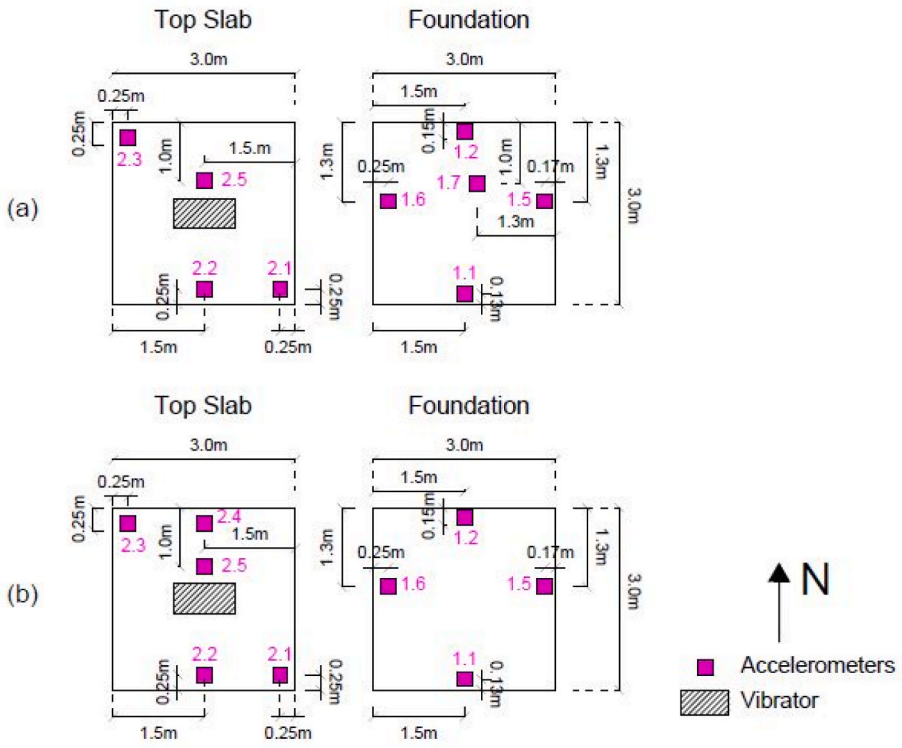

Fig. B.1. Plan views of the two structural instrument configurations

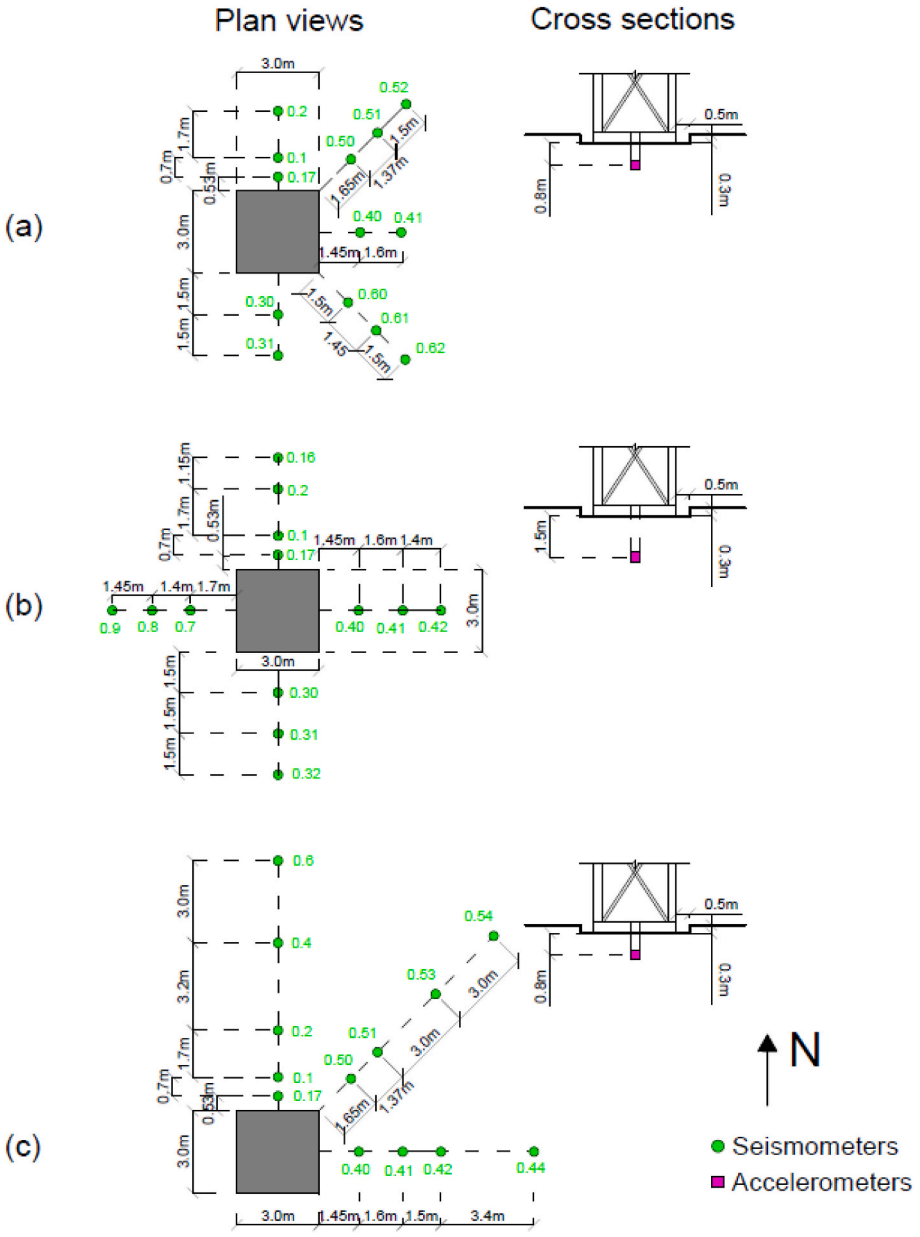

Fig. B.2. Plan views of the three configurations of soil instruments placed on the soil surface and downhole

Appendix C. Comparison of in-plane and out-of-plane experimental motions

Fig. C.1 compares the in and out-of-plane horizontal motions of the top slab, at the position of the 2.5 instrument, as produced by the forced vibration experiments: FBr_mD_5 Hz and PBr_mD_2 Hz. Fig. C2 compares the top slab response at the same location recorded by the free vibration experiments: FBr_2.9 kN, FBr_15.7 kN, PBr_2.0 kN and PBr_13.9 kN.

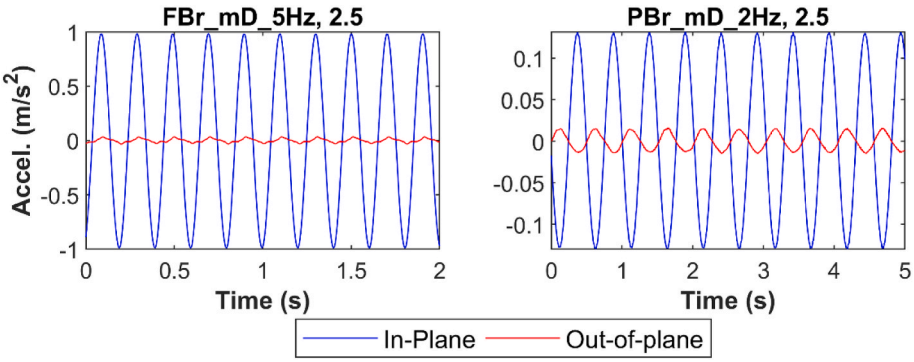

Fig. C.1. Comparison of top slab in-plane and out-of-plane motions recorded during the forced vibration tests, which were exploited in the present study

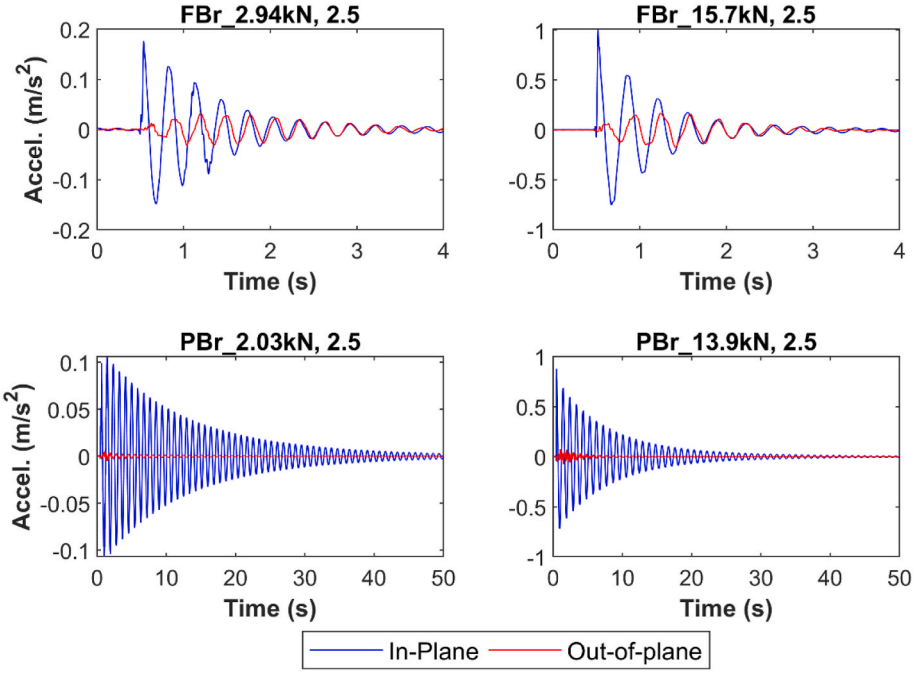

Fig. C.2. Comparison of the top slab in-plane and out-of-plane motions recorded during the free vibration tests, which were exploited in the presents study

References

[1] Pelekis I, McKenna F, Madabhushi GSP, DeJong MJ. Finite element modeling of buildings with structural and foundation rocking on dry sand. Earthq Eng Struct Dynam 2021;50:3093–115. https://doi.org/10.1002/eqe.3501.

[2] Raychowdhury P, Hutchinson TC. Performance evaluation of a nonlinear Winkler-based shallow foundation model using centrifuge test results. Earthq Eng Struct Dynam 2009;679–98. https://doi.org/10.1002/eqe.902.

[3] Maravas A, Mylonakis G, Karabalis DL. Simplified discrete systems for dynamic analysis of structures on footings and piles. Soil Dynam Earthq Eng 2014;61–62: 29–39. https://doi.org/10.1016/j.soildyn.2014.01.016.

[4] Stewart JP, Fenves GL, Seed RB. Seismic soil-structure interaction in buildings. I: analytical methods. J Geotech GEOENVIRONMENTAL Eng 1999;125:26–37.

[5] Pitilakis D, Dietz M, Wood DM, Clouteau D, Modaressi A. Numerical simulation of dynamic soil-structure interaction in shaking table testing. Soil Dynam Earthq Eng 2008;28:453–67. https://doi.org/10.1016/j.soildyn.2007.07.011.

[6] Bode C, Hirschauer R, Savidis SA. Soil-structure interaction in the time domain using halfspace Green's functions. Soil Dynam Earthq Eng 2002;22:283–95. https://doi.org/10.1016/S0267-7261(02)00020-9.

[7] Chao HY. Nonlinear dynamic soil-structure interaction analysis and application to lotung problem. 1996. https://doi.org/10.16953/deusbed.74839.

[8] Borja BRI, Chao H, Montans FJ, Lin C-H. SSI effects on ground motion at lotung LSST site. J Geotech GEOENVIRONMENTAL Eng 1999;125:760–70.

[9] Amorosi A, Boldini D, di Lernia A. Dynamic soil-structure interaction: three-dimensional numerical approach and its application to the Lotung case study. Comput Geotech 2017;90:34–54. https://doi.org/10.1016/j.compgeo.2017.05.016.

[10] Borja BRI, Amies AP. Multiaxial cyclic plasticity model for clay. J Geotech Eng 1994;120:1051–70.

[11] Schanz T, Vermeer PA, Bonnier PG. The hardening soil model: formulation and verification. Beyond 2000 in comput Geotech 1999;1:281–96.

[12] Benz T. Small-strain stiffness of soils and its numerical consequences. University of Stuttgart; 2007.

[13] Pitilakis D, Rovithis E, Massimino MR, Gatto MPA. Numerical simulation of large-scale soil-foundation-structure interaction experiments in the EuroProteas facility. Proc 6th Int Conf Earthq Geotech Eng 2015. https://doi.org/10.13140/RG.2.2.20002.43203.

[14] NIST. Soil-structure interaction for building structures. 2012. https://doi.org/10.22214/ijraset.2021.37763.

[15] Tileylioglu S, Stewart JP, Nigbor RL. Dynamic stiffness and damping of a shallow foundation from forced vibration of a field test structure. J Geotech Geoenviron Eng 2011;137:344–53. https://doi.org/10.1061/(asce)gt.1943-5606.0000430.

[16] Star LM, Givens MJ, Nigbor RL, Stewart JP. Field-testing of structure on shallow foundation to evaluate soil-structure interaction effects. Earthq Spectra 2015;31: 2511–34. https://doi.org/10.1193/052414EQS072.

[17] Stewart JP, Kim S, Bielak J, Dobry R, Power MS. Revisions to soil-structure interaction procedures in NEHRP design provisions. Earthq Spectra 2003;19: 677–96. https://doi.org/10.1193/1.1596213.

[18] Herrmann LR. Finite element analysis of contact problems. J Eng Mech Div 1979; 104:1043–57.

[19] Pande GN, Sharma KG. On joint/interface elements and associated problems of numerical ill-conditioning. Int J Numer Anal Methods GeoMech 1979;3:293–300. https://doi.org/10.1002/nag.1610030308.

[20] Griffiths DV. Numerical modelling of interfaces using conventional finite elements. pdf. 5th Int. Conf. Numer. Methods Geomech.; 1985. p. 837–44.

[21] Ghaboussi J, Wilson EL, Isenberg J. Finite element for RocK joints and interfaces. J Soil Mech Found Div 1973;99:833–48.
[22] Desai CS, Zaman MM, Lightner JG, Siriwardane HJ. THIN-LAYER element for interfaces and joints. Int J Numer Anal Methods GeoMech 1984;8:19–43.
[23] Zaman MM, Desai CS, Drumm EC. Interface model for dynamic soil-structure interaction. J Geotech Eng 1984;110:1257–73. https://doi.org/10.1061/(ASCE)0733-9410 (1987)113:5(537).
[24] Day RA, Potts DM. Zero thickness interface elements—numerical stability and application. Int J Numer Anal Methods GeoMech 1994;18:689–708. https://doi.org/10.1002/nag.1610181003.
[25] Gazetas G, Anastasopoulos I, Adamidis O, Kontoroupi T. Nonlinear rocking stiffness of foundations. Soil Dynam Earthq Eng 2013;47:83–91. https://doi.org/10.1016/j.soildyn.2012.12.011.
[26] Gazetas G. 4th Ishihara lecture: soil-foundation-structure systems beyond conventional seismic failure thresholds. Soil Dynam Earthq Eng 2015;68:23–39. https://doi.org/10.1016/j.soildyn.2014.09.012.
[27] Koronides M, Kontoe S, Zdravković L, Vratsikidis A, Pitilakis D, Anastasiadis A, et al. Numerical simulation of real-scale vibration experiments of a steel frame structure on a shallow foundation. In: Wang L, Zhang J-M, Wang R, editors. Proc. To 4th iInternational conf. Performance-Based des. Earthq. Eng. Beijing: Cham: Springer International Publishing; 2022. p. 1119–27.
[28] Koronides M, Kontoe S, Zdravković L, Vratsikidis A, Pitilakis D, Anastasiadis A, et al. Numerical simulations of field soil-structure interaction experiments on a shallow founded steel frame structure. Proc. to 3rd Int. Conf. Nat. Hazards Infrastruct. 2022;390.
[29] British Standards Institution. BS EN 1993-1-1:2005, Eurocode 3. Design of steel structures. General rules and rules for buildings; 2005.
[30] EKOS2000. Greek code for reinforced concrete. 2000.
[31] Pitilakis D, Anastasiadis A, Rovithis E, Manakou M, Riga E, Roumelioti Z, et al. Report on field testing for assessing input motions and SSI, Seismic engineering research infrastructures for european synergies. 2012.
[32] British standards institution. BS EN 1997-1:2004, Eurocode 7. Geotechnical design; 2004.
[33] Butterfield R, Gottardi G. A complete three-dimensional failure envelope for shallow footings on sand. Geotechnique 1994;44:181–4. https://doi.org/10.1680/geot.1994.44.1.181.
[34] Pitilakis K, Raptakis D, Lontzetidis K, Tika-Vassilikou T, Jongmans D. Geotechnical and geophysical description of euro-seistest, using field, laboratory tests and moderate strong motion recordings. J Earthq Eng 1999;3:381–409. https://doi.org/10.1080/13632469909350352.
[35] Pitilakis D, Rovithis E, Anastasiadis A, Vratsikidis A, Manakou M. Field evidence of SSI from full-scale structure testing. Soil Dynam Earthq Eng 2018;112:89–106. https://doi.org/10.1016/j.soildyn.2018.04.024.
[36] Raptakis D, Chávez-García FJ, Makra K, Pitilakis K. Site effects at Euroseistest-I. Determination of the valley structure and confrontation of observations with 1D analysis. Soil Dynam Earthq Eng 2000;19:1–22. https://doi.org/10.1016/S0267-7261(99)00025-1.
[37] Euroseistest Final Scientific Report. "Volvi-Thessaloniki a European test site for engineering seismology earthquake engineering and seismology" (Coordinator Pitilakis, K.). Pmject: EV5V - CT93 - 0281 (DIR 12 SOLS) 1995.
[38] Raptakis D, Makra K. Multiple estimates of soil structure at a vertical strong motion array: understanding uncertainties from different shear wave velocity profiles. Eng Geol 2015;192:1–18. https://doi.org/10.1016/j.enggeo.2015.03.016.
[39] Koronides M. Numerical and field investigation of dynamic soil structure interaction at full-scale. Imperial College London; 2023.
[40] Taborda DMG. Development of constitutive models for application in soil dynamics. Imperial College London; 2011.
[41] Guerreiro P, Kontoe S, Taborda D. Comparative study of stiffness reduction and damping curves. 15th World Conf Earthq Eng Lisbon Port 2012:2–11.
[42] Darendeli MB. Development of a new family of normalized modulus reduction and material damping curves. The University of Texas at Austin; 2001.
[43] Pitilakis K, Anastasiadis A, Pitilakis D, Rovithis E. Full-scale testing of a model structure in euroseistest to study soil-foundation-structure interaction. 4th ECCOMAS themat. Conf. Comput. Methods Struct. Dyn. Earthq. Eng. 2013: 1175–88. https://doi.org/10.7712/120113.4585.c1546.
[44] Givens MJ. Dynamic soil-structure interaction of instrumented buildings and test structures. UNIVERSITY OF CALIFORNIA Los Angeles; 2013.
[45] Tileylioglu. Evaluation of soil-structure interaction effects from field performance data. 2008.
[46] Potts DM, Zdravković L. Finite element analysis in geotechnical engineering: theory. London: Thomas Telford; 1999.
[47] Chung J, Hulbert GM. A time integration algorithm for structural dynamics with improved numerical dissipation: the generalized-α method. J Appl Mech 1993;60: 371–5. https://doi.org/10.1115/1.2900803.
[48] Kontoe S. Developement of time integration schemes and advanced boundary conditions for dynamic geotechnical analysis. Imperial College London; 2006.
[49] Han B, Zdravkovic L, Kontoe S. Stability investigation of the Generalised-α time integration method for dynamic coupled consolidation analysis. Comput Geotech 2015;64:83–95. https://doi.org/10.1016/j.compgeo.2014.11.006.
[50] Kuhlemeyer RL, Lysmer J. Finite element method accuracy for wave propagation problems. Soil Mech Found Div 1973;99:421–7.
[51] Kellezi L. Local transmitting boundaries for transient elastic analysis. Soil Dynam Earthq Eng 2000;19:533–47. https://doi.org/10.1016/S0267-7261(00)00029-4.
[52] Kontoe S, Zdravković L, Potts DM. An assessment of the domain reduction method as an advanced boundary condition and some pitfalls in the use of conventional absorbing boundaries. Int J Numer Anal Methods GeoMech 2009;33:309–30. https://doi.org/10.1002/nag.
[53] Gawecka KA, Potts DM, Cui W, Taborda DMG, Zdravković L. A coupled thermo-hydro-mechanical finite element formulation of one-dimensional beam elements for three-dimensional analysis. Comput Geotech 2018;104:29–41. https://doi.org/10.1016/j.compgeo.2018.08.005.
[54] Zienkiewicz OC, Bicanic N, Shen FQ. Earthquake input definition and the trasmitting boundary conditions. In: Doltsinis IS, editor. Adv. Comput. Nonlinear mech.; 1989. p. 109–38. https://doi.org/10.1007/978-3-7091-2828-2_3.
[55] British Standards Institution. BS EN 1992-1-1:2004. Eurocode 2. Design of concrete structures. General rules and rules for buildings; 2004.
[56] Woodward PK, Griffiths DV. Influence of viscous damping in the dynamic analysis of an earth dam using simple constitutive models. Comput Geotech 1996;19: 245–63. https://doi.org/10.1016/0266-352X(96)00002-X.
[57] Trifunac MD, Udwadia FE, Ba G. Analysis of errors in digitized strong-motion accelerograms. Bull Seismol Soc Am 1973;63:157–87.
[58] Iwan WD, Moser MA, Peng C-Y. Some observations on strong-motion earthquake measurement using a digital accelerograph. Bull Seismol Soc Am 1985;75: 1225–46. https://doi.org/10.1785/BSSA0750051225.
[59] Boore DM, Bommer JJ. Processing of strong-motion accelerograms: needs, options and consequences. Soil Dynam Earthq Eng 2005;25:93–115. https://doi.org/10.1016/j.soildyn.2004.10.007.
[60] Tan U, Veluvolu KC, Latt WT, Shee CY, Riviere CN, Ang WT. Estimating displacement of periodic motion with inertial sensors. IEEE Sensor J 2008;8: 1385–8.
[61] Jones J, Kalkan E, Stephens C, Ng P. PRISM software: processing and review interface for strong-motion data. Seismol Res Lett 2017;88:851–66. https://doi.org/10.1785/0220160200.
[62] Cui W, Potts DM, Zdravković L, Gawecka KA, Tsiampousi A. Formulation and application of 3D THM-coupled zero-thickness interface elements. Comput Geotech 2019;116:103204. https://doi.org/10.1016/j.compgeo.2019.103204.
[63] Potts DM, Zdravković L. Finite element analysis in geotechnical engineering: application. London: Thomas Telford Publishing; 2001. London.
[64] López AR, Tsiampousi A, Standing JR, Potts DM. Numerical investigation of a segmental grey cast iron tunnel ring: validation with laboratory data and application to field conditions. Comput Geotech 2022;141. https://doi.org/10.1016/j.compgeo.2021.104427.
[65] Taborda DMG, Potts DM, Zdravković L. On the assessment of energy dissipated through hysteresis in finite element analysis. Comput Geotech 2016;71:180–94. https://doi.org/10.1016/j.compgeo.2015.09.001.
[66] Measham PG, Taborda DMG, Zdravkovic L, Potts DM. Numerical simulation of a deep excavation in London Clay. Numer Methods Geotech Eng 2014;771–6. https://doi.org/10.1201/b17017-138.
[67] Kramer SL. Geotechnical earthquake engineering. New Jersey: Prentice Hall; 1996.
[68] Masing G. Eigenspannungen und verfestigung beim messing. 2nd Int. Conf. Appl. Mech. 1926:332–5.
[69] Amorosi A, Boldini D, Lernia A. Seismic ground response at Lotung: hysteretic elasto-plastic-based 3D analyses. Soil Dynam Earthq Eng 2016;85:44–61. https://doi.org/10.1016/j.soildyn.2016.03.001.
[70] Kaklamanos J, Baise LG, Thompson EM, Dorfmann L. Comparison of 1D linear, equivalent-linear, and nonlinear site response models at six KiK-net validation sites. Soil Dynam Earthq Eng 2015;69:207–19. https://doi.org/10.1016/j.soildyn.2014.10.016.
[71] Taborda DMG, Zdravkovic L. Application of a Hill-Climbing technique to the formulation of a new cyclic nonlinear elastic constitutive model. Comput Geotech 2012;43:80–91. https://doi.org/10.1016/j.compgeo.2012.02.001.
[72] Papaspiliou M, Kontoe S, Bommer JJ. An exploration of incorporating site response into PSHA-Part I: issues related to site response analysis methods. Soil Dynam Earthq Eng 2012;42:302–15. https://doi.org/10.1016/j.soildyn.2012.06.011.
[73] Phillips C, Hashash YMA. Damping formulation for nonlinear 1D site response analyses. Soil Dynam Earthq Eng 2009;29:1143–58. https://doi.org/10.1016/j.soildyn.2009.01.004.
[74] Han B. Hydro-mechanical coupling in numerical analysis of geotechnical structures under multi-directional seismic loading. Imperial College London; 2014.
[75] Korma E. The influence of advanced features of cyclic soil response on wave propagation problems. Imperial College London; 2014.
[76] Han B, Zdravkovic L, Kontoe S, Taborda DMG. Numerical investigation of the response of the Yele rockfill dam during the 2008 Wenchuan earthquake. Soil Dynam Earthq Eng 2016;88:124–42. https://doi.org/10.1016/j.soildyn.2016.06.002.
[77] Han B, Zdravkovic L, Kontoe S, Taborda DMG. Numerical investigation of multi-directional site response based on KiK-net downhole array monitoring data. Comput Geotech 2017;89:55–70. https://doi.org/10.1016/j.compgeo.2017.04.008.
[78] Chopra A. Dynamic of structures chopra. 2011.
[79] Gazetas G. Formulas and charts for impedances of surface and embedded foundations. J Geotech Eng 1991;117:1363–81.

[80] Gazetas G. Analysis of machine foundation vibrations: state of the art. Int J Soil Dynam Earthq Eng 1983;2:2–42. https://doi.org/10.1016/0261-7277(83)90025-6.

[81] Koronides M, Kontoe S, Zdravković L, Vratsikidis A, Pitilakis D, Anastasiadis A, et al. Numerical simulation of soil-structure interaction experiments on shallow founded structures for different mass configurations. In: Zdravkovic L, Kontoe S, Taborda DMG, Tsiampousi A, editors. 10th eur. Conf. Numer. Methods geotech. London: . Eng.; 2023.

[82] Salonikos T, Makarios T, Sous I, Lekidis V, Karakostas C. Design of instrumentation and vibration testing programs of structures through analytical investigations. Comput. methods Exp. Meas. XII. Malta 2005:579–88.